Copy 366
RM H58A30

NACA RM H58A30

NACA

RESEARCH MEMORANDUM

AN ANALYSIS OF SURFACE PRESSURES AND AERODYNAMIC LOAD DISTRIBUTION OVER THE SWEPT WING OF THE DOUGLAS D-558-II RESEARCH AIRPLANE AT MACH NUMBERS FROM 0.73 TO 1.73

By Norman V. Taillon

High-Speed Flight Station
Edwards, Calif.

CLASSIFICATION CHANGED TO UNCLASSIFIED
AUTHORITY: NASA TECHNICAL PUBLICATIONS ANNOUNCEMENTS NO. 48
EFFECTIVE DATE: MAY 29, 1961 WHL

CLASSIFIED DOCUMENT

This material contains information affecting the National Defense of the United States within the meaning of the espionage laws, Title 18, U.S.C., Secs. 793 and 794, the transmission or revelation of which in any manner to an unauthorized person is prohibited by law.

NATIONAL ADVISORY COMMITTEE
FOR AERONAUTICS

WASHINGTON

April 21, 1958

NATIONAL ADVISORY COMMITTEE FOR AERONAUTICS

RESEARCH MEMORANDUM

AN ANALYSIS OF SURFACE PRESSURES AND AERODYNAMIC LOAD DISTRIBUTION OVER THE SWEPT WING OF THE DOUGLAS D-558-II RESEARCH AIRPLANE AT MACH NUMBERS FROM 0.73 TO 1.73

By Norman V. Taillon

SUMMARY

This paper presents the wing-section pressure-distribution and wing-panel load characteristics of the Douglas D-558-II airplane for Mach numbers from about 0.73 to approximately 1.73 and for airplane normal-force coefficients from about 0 to approximately 0.8.

At subsonic speeds the pressure distributions are characterized by a high negative-pressure peak with an abrupt pressure recovery as a result of the leading-edge expansion over the upper surface at moderate angles of attack.

The shapes of the lower surface pressure distributions show little change with increases in angle of attack. At supersonic speeds the upper surface chordwise pressures approach a uniform distribution at the higher angles of attack. The spanwise lift distribution is nearly elliptical under all conditions, except for a distortion in the transonic range caused by shock movement and tip-separation effects. Comparisons of the spanwise loading with theory at a moderate lift coefficient show good agreement at subsonic Mach numbers; however, at supersonic speeds theory predicted a center of pressure nearer the wing tip.

The chordwise center of pressure ranges from about 20-percent chord at Mach numbers below 0.80 to about 40-percent chord at Mach numbers greater than 1.0. The spanwise center of pressure moves from about 43-percent panel span to about 45-percent panel span at similar Mach numbers. An excursion above the stability boundary at a Mach number of 0.9 results in extensive separation starting at the wing tip. This separation causes a loss of lift at the outboard stations and a reduction of lift-curve slope for the inboard stations, thus initiating an inboard and forward movement of the wing-panel center of pressure.

INTRODUCTION

Flight tests of the Douglas D-558-II research airplane have been conducted by the NACA High-Speed Flight Station at Edwards, Calif., to explore the characteristics in flight of an airplane with a moderately swept wing at speeds up to a Mach number of 2.0. As part of this investigation the aerodynamic characteristics of the wing were determined by upper and lower surface pressure measurements. Chordwise and spanwise load distributions in the transonic region at low lift have been reported in reference 1, and section characteristics at a midsemispan station up to the maximum Mach number of 2.0 were reported in reference 2. The present paper presents more complete wing pressure-distribution and loads data than have been published previously for the D-558-II airplane.

The data presented provide surface-pressure and load-distribution information at Mach numbers from 0.73 to 1.73 for a moderately swept wing with a subsonic-type airfoil.

SYMBOLS

$b/2$ wing-panel span, spanwise distance from wing station 38 (orifice row 6) to wing tip, 9.25 ft

C_N wing-panel normal-force coefficient, $\int_0^1 c_n \frac{c}{c_{av}} d\frac{2y}{b}$

$C_{N_\alpha} = \frac{dC_{N_A}}{d\alpha}$ or $\frac{dC_N}{d\alpha}$

C_{N_A} airplane normal-force coefficient

C_b wing-panel bending-moment coefficient about wing station 38, $\int_0^1 c_n \frac{c}{c_{av}} \frac{2y}{b} d\frac{2y}{b}$

C_m wing-panel pitching-moment coefficient about $0.25\bar{c}$, $\frac{c_{av}}{\bar{c}} \int_0^1 c_m \left(\frac{c}{c_{av}}\right)^2 d\frac{2y}{b}$

C_p pressure coefficient, $\frac{p - p_0}{q}$

c local wing chord parallel to plane of symmetry, ft

$\bar{c}$ mean aerodynamic chord of wing panel, $2/S \int_0^{b/2} c^2 dy$

c' local wing chord normal to 30-percent common-chord line

c_{av} average chord of wing panel parallel to plane of symmetry, 6.475 ft

c_m section pitching-moment coefficient about line perpendicular to longitudinal axis of airplane passing through $0.25\bar{c}$

$c_{m'}$ section pitching-moment coefficient about $0.25c'$, $\int_0^1 \frac{p_l - p_u}{q}\left(0.25 - \frac{x'}{c'}\right) d\frac{x'}{c'}$

c_n section normal-force coefficient parallel to plane of symmetry, $\int_0^1 \frac{p_l - p_u}{q} d\frac{x}{c}$

$c_{n'}$ section normal-force coefficient normal to 30-percent common-chord line, $\int_0^1 \frac{p_l - p_u}{q} d\frac{x'}{c'}$

M free-stream Mach number

p local static pressure, lb/sq ft

p_l local static pressure on lower wing surface, lb/sq ft

p_0 free-stream static pressure, lb/sq ft

p_u local static pressure on upper wing surface, lb/sq ft

q free-stream dynamic pressure, lb/sq ft

$S/2$ area of one wing panel outboard of wing station 38, 60.435 sq ft

x distance rearward of leading edge of local chord parallel to plane of symmetry, ft

x' distance rearward of leading edge of local chord normal to 30-percent common chord, ft

x_{cp} wing-panel chordwise center of pressure, percent $\bar{c}$

x'_{cp} section chordwise center of pressure, percent c'

y spanwise distance outboard of wing station 38, ft

y_{cp} wing-panel lateral center of pressure, percent b/2

α airplane angle of attack, deg

DESCRIPTION OF AIRPLANE AND WING PANEL

The research airplane used for this investigation is an all-rocket version of the D-558-II series. A photograph of the airplane is shown in figure 1, and a three-view drawing with the major dimensions is presented in figure 2. Dimensions and physical characteristics are given in table I.

The wing is swept back 35° at the 30-percent common-chord line and has a taper ratio of 0.565, an aspect ratio of 3.57, and 3° of incidence. The wing airfoil sections normal to the 30-percent common-chord line are NACA 63-010 at the root and NACA 63_1-012 at the tip resulting in streamwise thicknesses of 8.7 percent at the root and 10.4 percent at the tip. Ordinates of the root and tip airfoils are presented in tables II and III, respectively. The leading-edge slat was permanently secured in the closed position and faired-in with filler putty to form a smooth airfoil surface for these tests.

A drawing of the wing showing orifice row locations is given in figure 3. The wing panel is defined as that portion of the wing outboard of wing station 38 (orifice station A). The chordwise location of each orifice is given in table IV. It may be noted that four orifice rows are located perpendicular to the 30-percent common-chord line, and two orifice stations (at root and tip) are parallel to the plane of symmetry.

INSTRUMENTATION AND ACCURACY

Standard NACA instruments were installed in the airplane to record the following measurements pertinent to this investigation:

Wing pressures
Airspeed and altitude
Airplane angle of attack and angle of sideslip
Normal acceleration at the airplane center of gravity
Left aileron position
Rolling velocity and acceleration
Pitching velocity and acceleration

All instruments were synchronized by a common timer.

Flush-type orifices installed in the wing skin were connected by tubing to NACA 24-cell recording manometers. An NACA high-speed pitot-static tube was mounted on a boom which projected from the nose of the airplane. Angle-of-attack and angle-of-yaw vanes were also located on the boom. The maximum estimated error in angle of attack, based on estimates of the recording accuracy, boom bending, upwash, and vane floating, is about 1°. Estimated maximum errors of the other quantities pertinent to this investigation are:

M	± 0.02
C_{N_A}	± 0.02
C_p	± 0.03
c_n'	± 0.04
c_m'	± 0.01
C_N	± 0.05
C_m	± 0.02

TESTS

Wing-pressure-distribution data were recorded during a series of pull-ups through the speed range from $M \approx 0.73$ to $M \approx 1.73$ at altitudes between 25,000 and 60,000 feet. Lag in the wing pressure-recording system was negligible for the slow-rate maneuvers performed. The angle-of-attack range presented for subsonic and transonic speeds is generally limited to moderate values because of the high pitching rates encountered above the stability boundary. However, data were obtained at high lift at $M = 0.9$ during one excursion above the stability boundary in which low pitching rates were involved.

DATA REDUCTION AND PRESENTATION

The arrangement of orifices on the wing of the D-558-II airplane is shown in figure 3. As previously noted, the orifice rows were oriented in two planes: Perpendicular to the 30-percent common-chord line (rows 1 to 4), and parallel to the plane of symmetry, or streamwise (stations A and F). In order to obtain the integrated wing-panel characteristics, requiring chordwise pressure distributions parallel to the plane of symmetry, the chordwise pressures for stations B to E were obtained by constructing spanwise pressure plots from the measured data and selecting the faired values at the locations of the streamwise stations. The same technique was used to obtain the pressure distribution for the forward 35 percent of station F where measured data were not available.

For the data presented angular velocities and accelerations, angle of sideslip, and aileron deflection were small and have been neglected.

All the data obtained during the investigation are available in tabulated form, upon request, from the National Advisory Committee for Aeronautics.

RESULTS AND DISCUSSION

Pressure Distribution

The measured chordwise pressure distributions are superimposed on the wing plan form in figures 4 and 5. Upper and lower surface pressures are designated by solid and broken lines, respectively. Alternate stations have been shaded for greater clarity. Figure 4 presents the variation of the wing pressure distribution with lift at constant Mach numbers, and figure 5 presents the variation with Mach number at constant airplane lift. These figures are supplemented by the pressure-contour charts of figure 6 which were constructed from the data of figures 4 and 5.

At subsonic speeds (fig. 4(a)) an increase in angle of attack serves to develop the upper surface triangular chordwise pressure distribution typical of subsonic loading. The shape of the lower surface pressure distributions remains nearly the same throughout the airplane normal-force range.

In the transonic range, illustrated by figures 4(b) to 4(d), shocks are indicated at low lift by an abrupt pressure recovery, but are obscure at high lift. Some separation is evident on the upper surface, particularly near the tip at high lift at $M \approx 0.9$.

At supersonic Mach numbers ($M \approx 1.48$ and $M \approx 1.73$) the upper surface chordwise pressures approach a uniform distribution at the higher angles of attack.

Figure 5 illustrates more clearly the effect of Mach number on the pressure distribution at low lift $\left(C_{N_A} \approx 0.2\right)$. At $M = 0.74$ the subsonic leading-edge-pressure peak causes the loading to be well forward at each chordwise station.

The pressure distribution at $M = 0.90$ shows an erratic variation along the span caused by a reduction in the leading-edge pressure peak and the formation of a strong shock wave diagonally across the wing panel. In addition to the well-developed compression shock on the upper surface approximately perpendicular to the fuselage, a somewhat lesser shock has developed on the lower surface. The chordwise position of the upper-surface shock at low lift and at $M \approx 0.90$ is clearly evident from the steep pressure gradient on the pressure-contour plot of this condition in figure 6(b). With an increase in Mach number to 1.00 it may be seen that the shock sweeps rearward, becoming more nearly parallel to the trailing edge.

The superimposed pressure plots and pressure contours for $M \approx 1.48$ and $M \approx 1.73$ show that the shock wave is at the trailing edge and that a nearly uniform pressure distribution exists over the upper surface of the wing.

Aerodynamic Characteristics of the Wing Section

The variation of section normal-force coefficient with airplane angle of attack is presented for orifice rows 1 to 4 (normal to the 30-percent chord line) in figure 7. It may be noted that at a Mach number of about 0.90 the outboard rows (3 and 4) show a loss of lift and the inboard rows (1 and 2) exhibit a reduction in slope at the higher angles of attack where extensive separation is present. A reduction in slope is also apparent for some rows at transonic Mach numbers. The outboard rows have a lower lift-curve slope than the root row at $M \approx 0.73$, and row 4 (nearest the tip) is nonlinear throughout the transonic range. At Mach numbers greater than about 1.1 the lift-curve slopes of the four rows are about equal.

Figure 8 presents the variation of section pitching-moment coefficient with section normal-force coefficient at rows 1 to 4 throughout the Mach number range. Except for the transonic region, the curves are linear; however, the slope changes from a neutral or slightly positive pitching moment at subsonic Mach numbers to a negative value at supersonic Mach numbers as the chordwise center of pressure moves rearward.

The effect of Mach number on the chordwise center of pressure of the four rows at airplane lift coefficients of about 0.2, 0.4, and 0.6 is shown in figure 9. It may be noted that for a Mach number of 0.8 the center of pressure is more forward for the outboard rows. As Mach number increases from about 0.85 to 0.90, there is a rapid rearward movement of the center of pressure. This movement stabilizes at about 40-percent chord of each row, where it remains to the highest Mach number tested.

Aerodynamic Characteristics of the Wing Panel

The spanwise load and pitching-moment distributions are presented in figures 10 and 11, respectively, to show the effect of lift over the Mach number range from 0.73 to 1.73.

At all Mach numbers a reduction in loading is evident at low lift near the root, apparently as a result of fuselage interference effects. In this connection, it may be noted that the wing has 3° incidence. At moderate angles of attack the loss in lift near the root becomes less noticeable.

At subsonic Mach numbers (0.73 and 0.82) the span loadings are nearly elliptical in shape except near the root, and lift has a negligible effect on the shape of the load and pitching-moment distributions. In the transonic region (Mach numbers of 0.9 to 1.1) there is some distortion in the spanwise load distribution due to shock movement, and, in addition, a loss of lift and a reduction in pitching moment occur near the wing tip as a result of the previously mentioned tip-separation effects. At supersonic Mach numbers the loading again becomes elliptic, and the shapes of both the loading and pitching-moment distributions are much like their subsonic counterparts. Theoretical wing-panel spanwise-load distributions have been calculated for comparison with flight loads at a nominal panel normal-force coefficient of 0.4 and Mach numbers of 0.73, 1.48, and 1.73 by employing the Weissinger method (ref. 3) and linear theory (ref. 4) for the subsonic and supersonic speeds, respectively. The calculated curves are shown by broken lines in figures 10(a), 10(h), and 10(i). At subsonic speeds the agreement between theory and flight data for this lift coefficient is generally good, with some disagreement near the root. Because of the reduction in loading near the root the agreement would obviously be poorer at lower lift. At supersonic speeds, for the lift coefficient shown, theory predicts a center of loading nearer the wing tip, a departure from the more nearly elliptical loading obtained in flight. The agreement between theory and flight data would be somewhat better at the lower lift coefficients.

Figure 12 shows the variation of panel normal-force coefficient with angle of attack throughout the Mach number range. The curves are essentially linear through the lift range at the Mach numbers selected (except

at $M \approx 0.90$) with a reduction in slope at supersonic Mach numbers. The result of high-lift flow separation at $M \approx 0.90$ is clearly visible in this figure.

In figure 13 it may be seen that the variation of panel bending-moment coefficient with panel lift coefficient is nearly constant for the Mach number range tested. The variation of panel pitching-moment coefficient with panel normal-force coefficient is presented in figure 14. At the lower Mach numbers the slopes of the pitching-moment curves are approximately neutral, but as Mach number increases they become negative. The positive slope at the higher normal-force coefficients at $M \approx 0.90$ is a result of the separation at the outboard stations discussed earlier.

The center-of-pressure locations, as illustrated in figure 15, show that the chordwise position varies from about 20-percent chord at Mach numbers below 0.8 to about 40-percent chord at Mach numbers greater than 1.0. The spanwise position varies from about 43-percent wing-panel span at Mach numbers below 0.8 to about 45-percent wing-panel span at Mach numbers greater than 1.0. Comparison of theoretical y_{cp} for a C_{N_A} of 0.4 shows good agreement with flight results at subsonic speeds, but poor agreement at supersonic speeds.

The variations of the airplane and wing-panel normal-force-curve slopes $\left(C_{N_\alpha}\right)$ with Mach number are shown in figure 16. The slopes increase from about 0.07 at subsonic speeds to a maximum of about 0.09 at $M = 0.90$ for the airplane, and at $M = 1.00$ for the wing panel; thereafter, the slopes decrease to a value of about 0.05 at $M = 1.73$, illustrating the loss of lifting efficiency within the supersonic region. Theoretical wing-panel normal-force-curve slopes at Mach numbers of 0.73, 1.50, and 1.73 computed using references 3 to 5 show good agreement with flight results.

CONCLUSIONS

An analysis of section and wing-panel pressure distributions and loads obtained in a series of pull-ups performed with the D-558-II research airplane at Mach numbers from 0.73 to 1.73 indicated that:

1. At subsonic speeds the upper surface pressure distributions were characterized by a high negative-pressure peak as a result of leading-edge expansion at moderate angles of attack. The lower surface pressure distributions showed little change in shape with changes in angle of attack. At supersonic speeds the upper surface chordwise loading approached a uniform distribution at the higher angles of attack.

2. The spanwise lift distributions were nearly elliptical except near the root at subsonic and supersonic Mach numbers, with a distortion in the transonic range caused by shock movement and tip-separation effects. For the lift coefficient at which comparisons with theory were made theory showed good agreement at subsonic Mach numbers. However, theory predicted a center of pressure nearer the wing tip at supersonic speeds.

3. The wing center-of-pressure location ranged from about 20-percent chord and 43-percent panel span at Mach numbers below 0.80 to about 40-percent chord and 45-percent panel span at Mach numbers greater than 1.0.

4. Extensive separation above the stability boundary at a Mach number of 0.90 caused a loss of lift at the outboard stations and a reduction of lift-curve slope at the inboard stations, resulting in an inboard and forward movement of the center of pressure. A reduction of slope also occurred at the higher lifts attained at other transonic Mach numbers.

High-Speed Flight Station,
National Advisory Committee for Aeronautics,
Edwards, Calif., January 10, 1958.

REFERENCES

1. Peele, James R.: Flight-Determined Pressure Measurements Over the Wing of the Douglas D-558-II Research Airplane at Mach Numbers up to 1.14. NACA RM L54A07, 1954.

2. Jordan, Gareth H., and Keener, Earl R.: Flight-Determined Pressure Distributions Over a Section of the 35° Swept Wing of the Douglas D-558-II Research Airplane at Mach Numbers up to 2.0. NACA RM H55A03, 1955.

3. De Young, John, and Harper, Charles W.: Theoretical Symmetric Span Loading at Subsonic Speeds for Wings Having Arbitrary Plan Form. NACA Rep. 921, 1948.

4. Martin, John C., and Jeffreys, Isabella: Span Load Distributions Resulting From Angle of Attack, Rolling, and Pitching for Tapered Sweptback Wings With Streamwise Tips. Supersonic Leading and Trailing Edges. NACA TN 2643, 1952.

5. Mangler, K. W.: Calculation of the Pressure Distribution Over a Wing at Sonic Speeds. R. & M. No. 2888, British A.R.C., Sept. 1951.

TABLE I.- DIMENSIONS AND CHARACTERISTICS OF THE

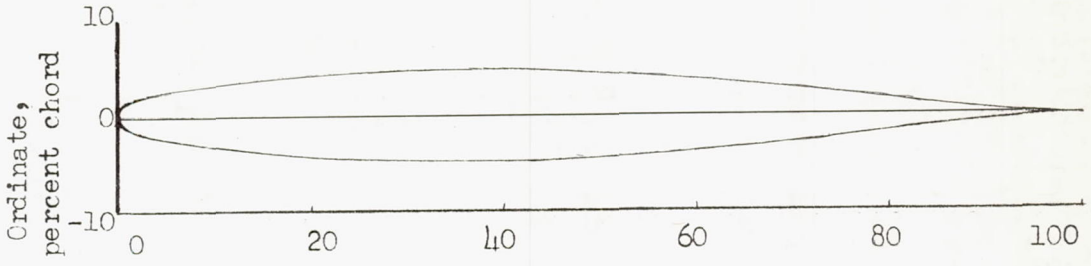
DOUGLAS D-558-II AIRPLANE

Wing:	
Root airfoil section (normal to 30-percent chord of unswept panel)	NACA 63-010
Tip airfoil section (normal to 30-percent chord of unswept panel)	NACA 63_1-012
Total area, sq ft	175.0
Span, ft	25.0
Mean aerodynamic chord, in.	87.301
Root chord (parallel to plane of symmetry), in.	108.51
Extended tip chord (parallel to plane of symmetry), in.	61.18
Taper ratio	0.565
Incidence, deg	3.0
Aspect ratio	3.570
Sweep at 30-percent chord of unswept panel, deg	35.0
Sweep of leading edge, deg	38.8
Dihedral, deg	-3.0
Geometric twist, deg	0
Horizontal tail:	
Root airfoil section (normal to 30-percent chord of unswept panel)	NACA 63-010
Tip airfoil section (normal to 30-percent chord of unswept panel)	NACA 63-010
Total area, sq ft	39.9
Span, in.	143.6
Mean aerodynamic chord, in.	41.75
Root chord (parallel to plane of symmetry), in.	53.6
Extended tip chord (parallel to plane of symmetry), in.	26.8
Taper ratio	0.50
Aspect ratio	3.59
Sweep at 30-percent-chord line of unswept panel, deg	40.0
Dihedral, deg	0
Vertical tail:	
Airfoil section (parallel to fuselage center line)	NACA 63-010
Effective area (area above root chord), sq ft	36.6
Height from fuselage center line, in.	98.0
Root chord (parallel to fuselage center line), in.	146.0
Extended tip chord (parallel to fuselage center line), in.	44.0
Sweep angle at 30-percent chord of unswept panel, deg	49.0
Fuselage:	
Length, ft	42.0
Maximum diameter, in.	60.0
Fineness ratio	8.40
Power plant:	
Rocket	LR8-RM-6
Airplane weight, lb:	
Full rocket fuel	15,787
No fuel	9,421

TABLE II.- PROFILE AND ORDINATES OF ROOT SECTION

(NACA 63-010 AIRFOIL)

[Stations and ordinates given in percent of local chord]

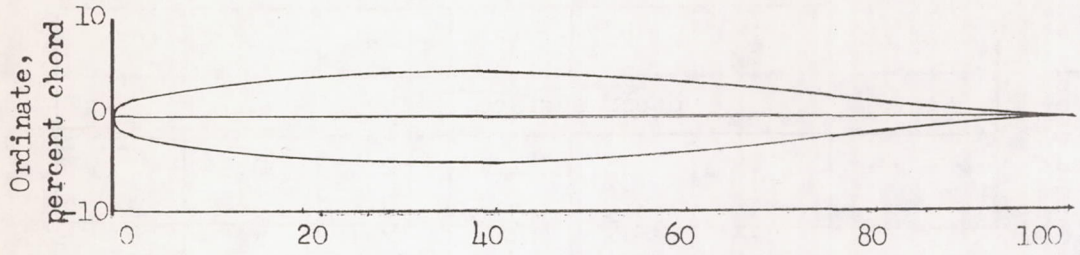


Station	Upper surface	Lower surface
0	0	0
.5	.829	-.829
.75	1.004	-1.004
1.25	1.275	-1.275
2.5	1.756	-1.756
5.0	2.440	-2.440
7.5	2.950	-2.950
10	3.362	-3.362
15	3.994	-3.994
20	4.445	-4.445
25	4.753	-4.753
30	4.938	-4.938
35	5.000	-5.000
40	4.938	-4.938
45	4.766	-4.766
50	4.496	-4.496
55	4.140	-4.140
60	3.715	-3.715
65	3.234	-3.234
70	2.712	-2.712
75	2.166	-2.166
80	1.618	-1.618
85	1.088	-1.088
90	.604	-.604
95	.214	-.214
100	0	0
L.E. radius: 0.770		

TABLE III.- PROFILE AND ORDINATES OF TIP SECTION

(NACA 63_1-012 AIRFOIL)

[Stations and ordinates given in percent of local chord]



Station	Upper surface	Lower surface
0	0	0
.5	.985	-.985
.75	1.194	-1.194
1.25	1.519	-1.519
2.5	2.102	-2.102
5.0	2.925	-2.925
7.5	3.542	-3.542
10	4.039	-4.039
15	4.799	-4.799
20	5.342	-5.342
25	5.712	-5.712
30	5.930	-5.930
35	6.000	-6.000
40	5.920	-5.920
45	5.704	-5.704
50	5.370	-5.370
55	4.935	-4.935
60	4.420	-4.420
65	3.840	-3.840
70	3.210	-3.210
75	2.556	-2.556
80	1.902	-1.902
85	1.274	-1.274
90	.707	-.707
95	.250	-.250
100	0	0
L.E. radius: 1.087		

TABLE IV.- LOCATION OF ORIFICES ON THE WING OF THE D-558-II AIRPLANE

Orifice / Row or station	Orifice location, percent of local chord					
	1	2	3	4	A	F
Upper surface						
2	1.2	1.3	1.1	1.3	0.9	31.5
4	2.5	2.6	2.3	5.2	3.3	34.1
6	4.1	4.9	5.0	19.7	4.9	39.6
8	9.1	9.0	8.2	31.4	10.0	43.5
10	19.0	19.4	18.6	35.2	21.1	50.1
12	31.0	31.2	30.8	39.8	34.7	55.0
14	35.3	35.0	34.7	44.1	39.7	59.8
16	40.1	51.1	39.4	55.2	44.2	64.1
18	44.1	55.0	50.8	60.4	50.2	71.3
20	51.4	59.9	60.0	64.0	55.3	80.3
22	55.2	63.8	62.8	69.3	59.1	86.1
24	60.8	70.8	85.4	76.0	64.4	90.0
26	62.7	75.6	89.5	79.8	70.3	94.8
28	71.3	80.1	95.2	85.7	78.2	
30	75.1	85.0		94.9		
32	80.6	89.8				
34	86.0	94.7				
36	90.0					
38	95.2					
Lower surface						
3	0.6	0.8	0.7	0.7	0.8	31.4
5	3.1	3.6	5.9	6.1	3.0	34.2
7	5.6	5.8	11.1	10.7	5.3	47.3
9	10.6	11.1	19.0	30.8	9.8	50.6
11	30.5	18.9	31.1	33.5	43.5	55.6
13	39.6	30.9	34.8	38.9	50.2	60.0
15	43.5	34.5	40.1	44.5	59.8	64.8
17	50.5	50.8	51.1	55.2	70.8	72.0
19	54.4	56.3	55.0	60.2	74.8	79.1
21	59.6	59.9	60.0	64.2	77.8	86.1
23	63.6	63.9	63.0	71.1	90.0	90.2
25	70.6	70.7	85.4	75.9	95.0	95.2
27	74.6	75.3	89.5	79.9		
29	79.8	84.8	95.0	85.8		
31	85.4	94.4		89.7		
33	89.6					
35	94.7					

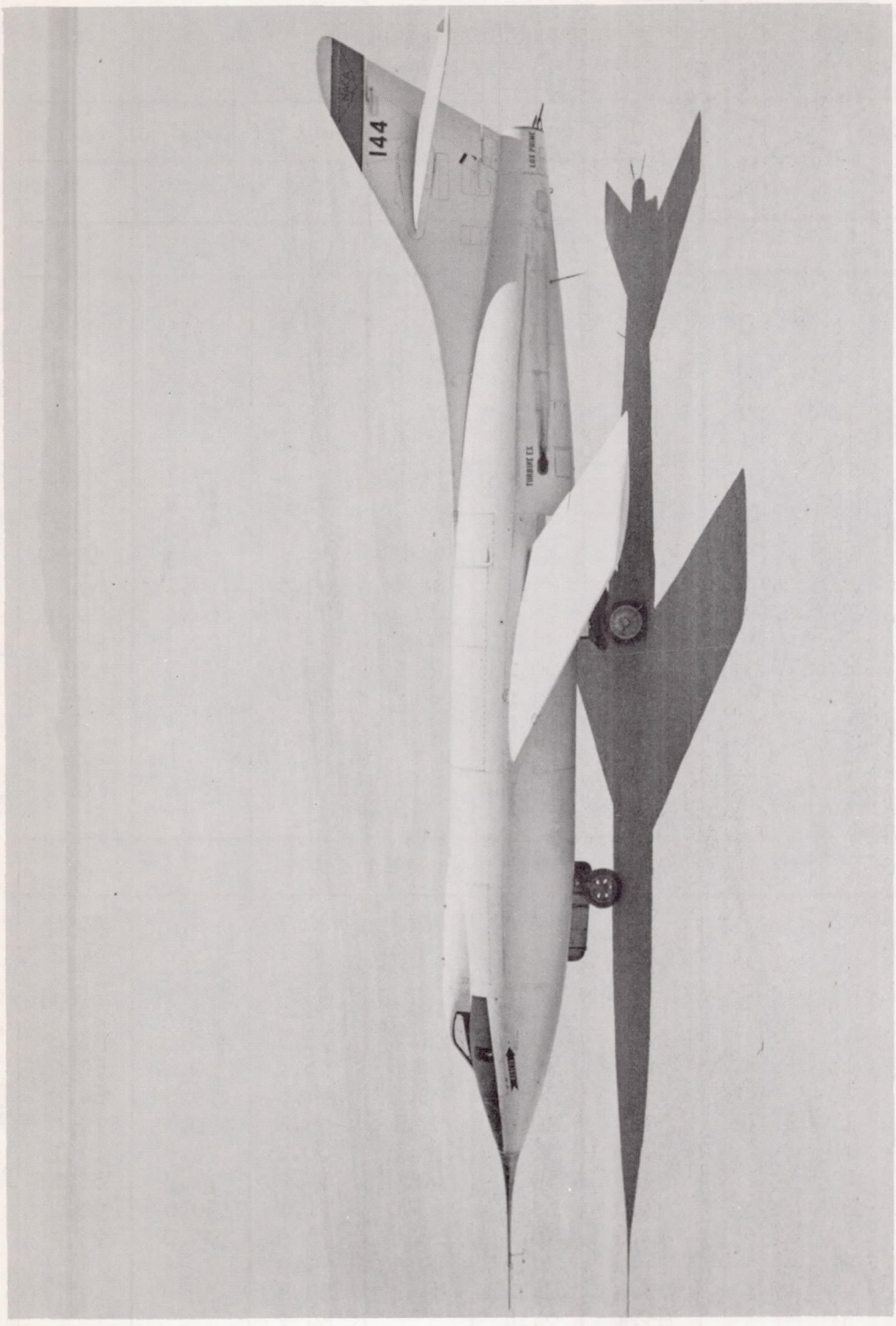


Figure 1.- Photograph of the D-558-II (144) research airplane. E-2895

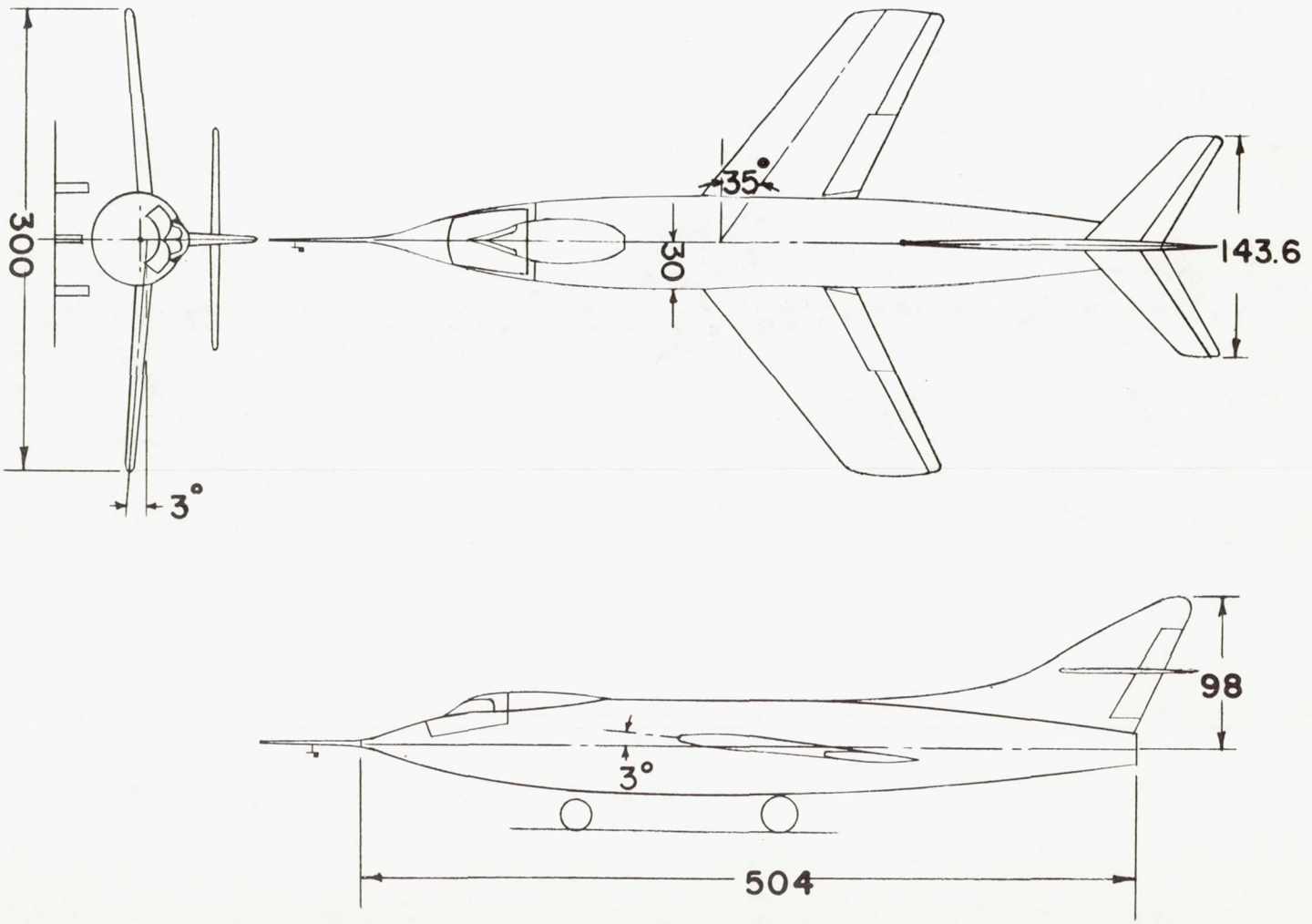
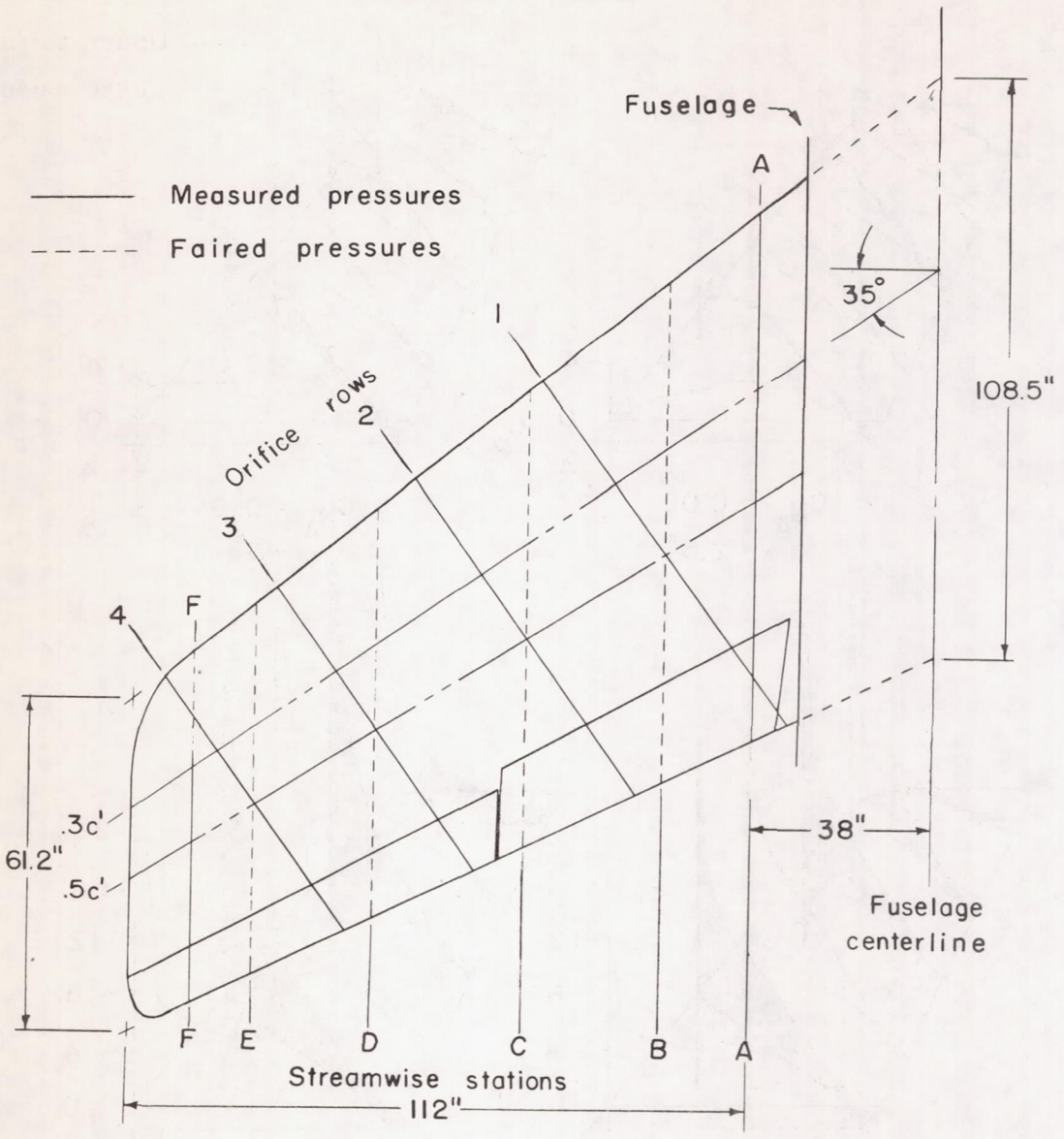
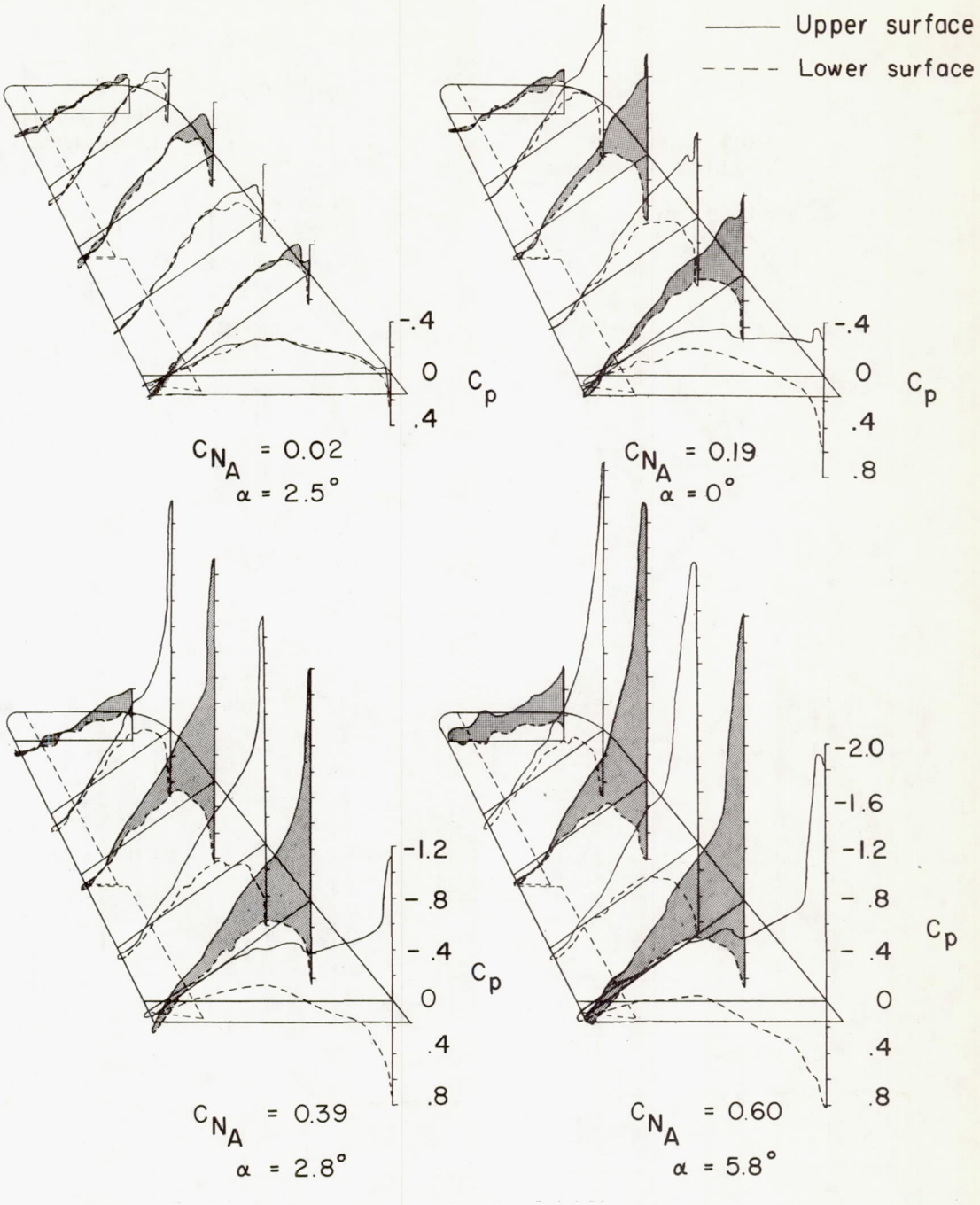


Figure 2.- Three-view drawing of the Douglas D-558-II airplane. All dimensions in inches.



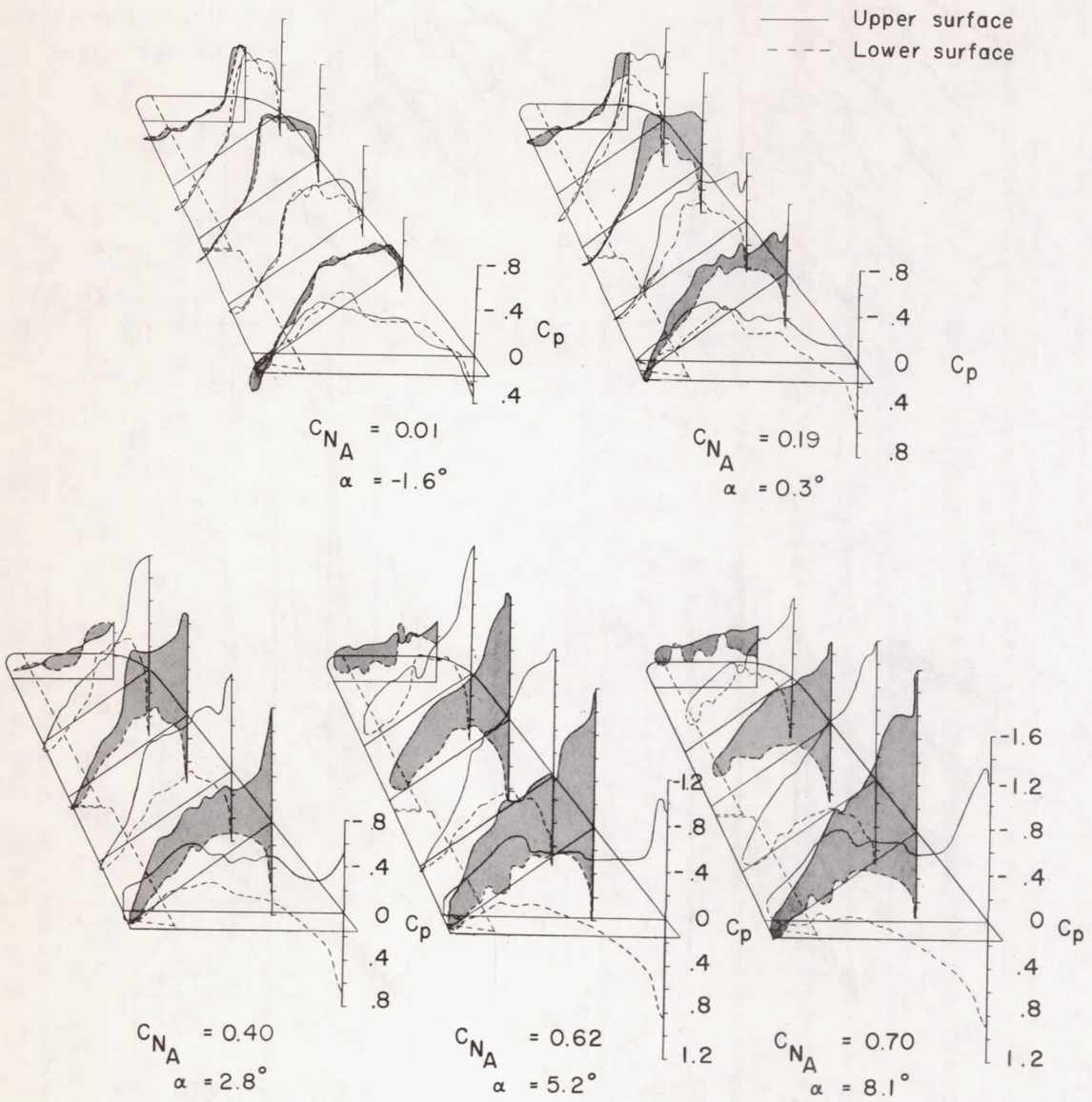
Streamwise station	A	B	C	D	E	F
Spanwise location, percent b/2	0	15	35.5	60	79.4	90.2

Figure 3.- Wing of the D-558-II airplane showing orifice rows and spanwise stations.



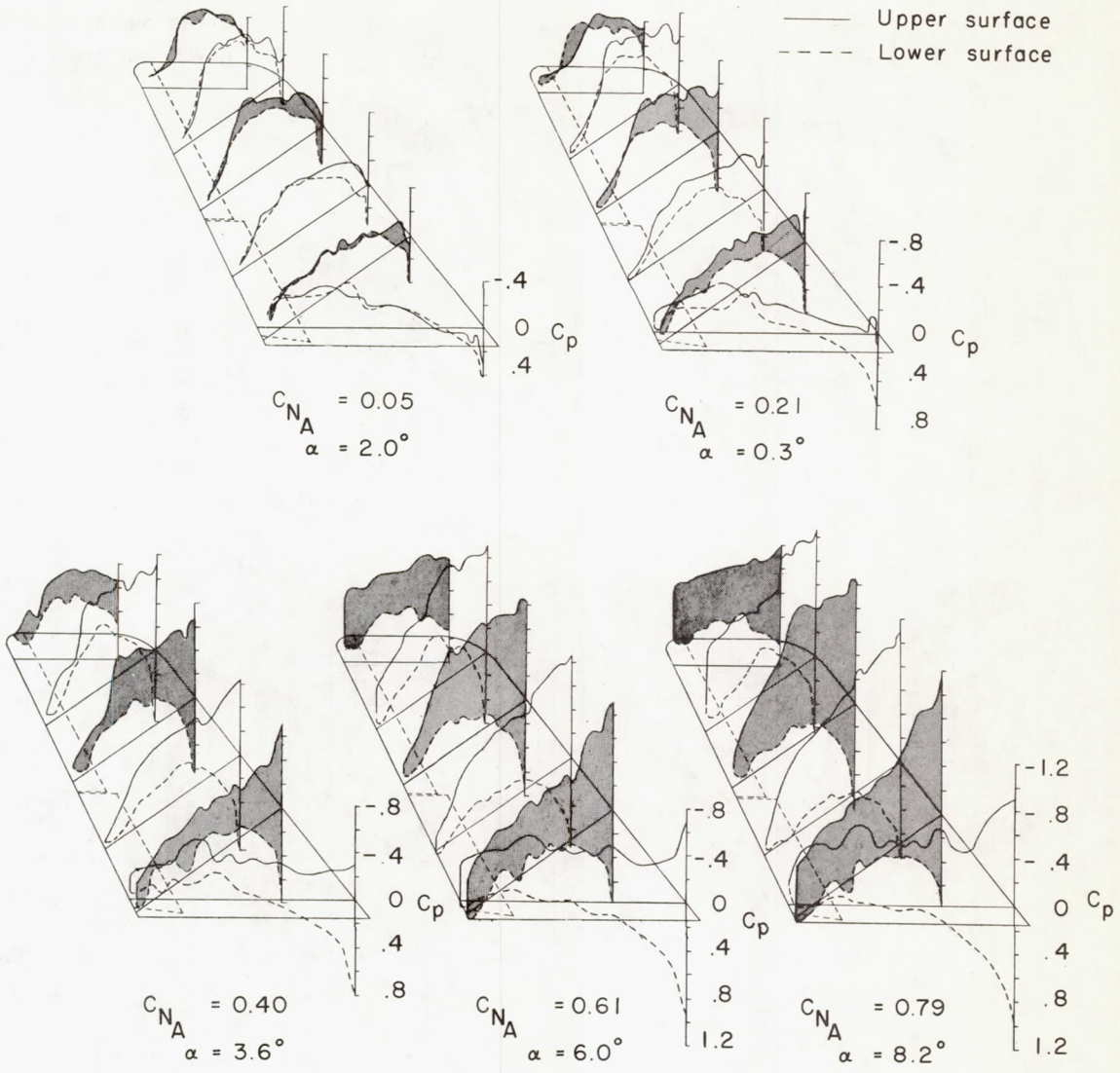
(a) M ≈ 0.73.

Figure 4.- Wing plan views showing the effect of lift on the D-558-II wing pressure distributions at representative Mach numbers.



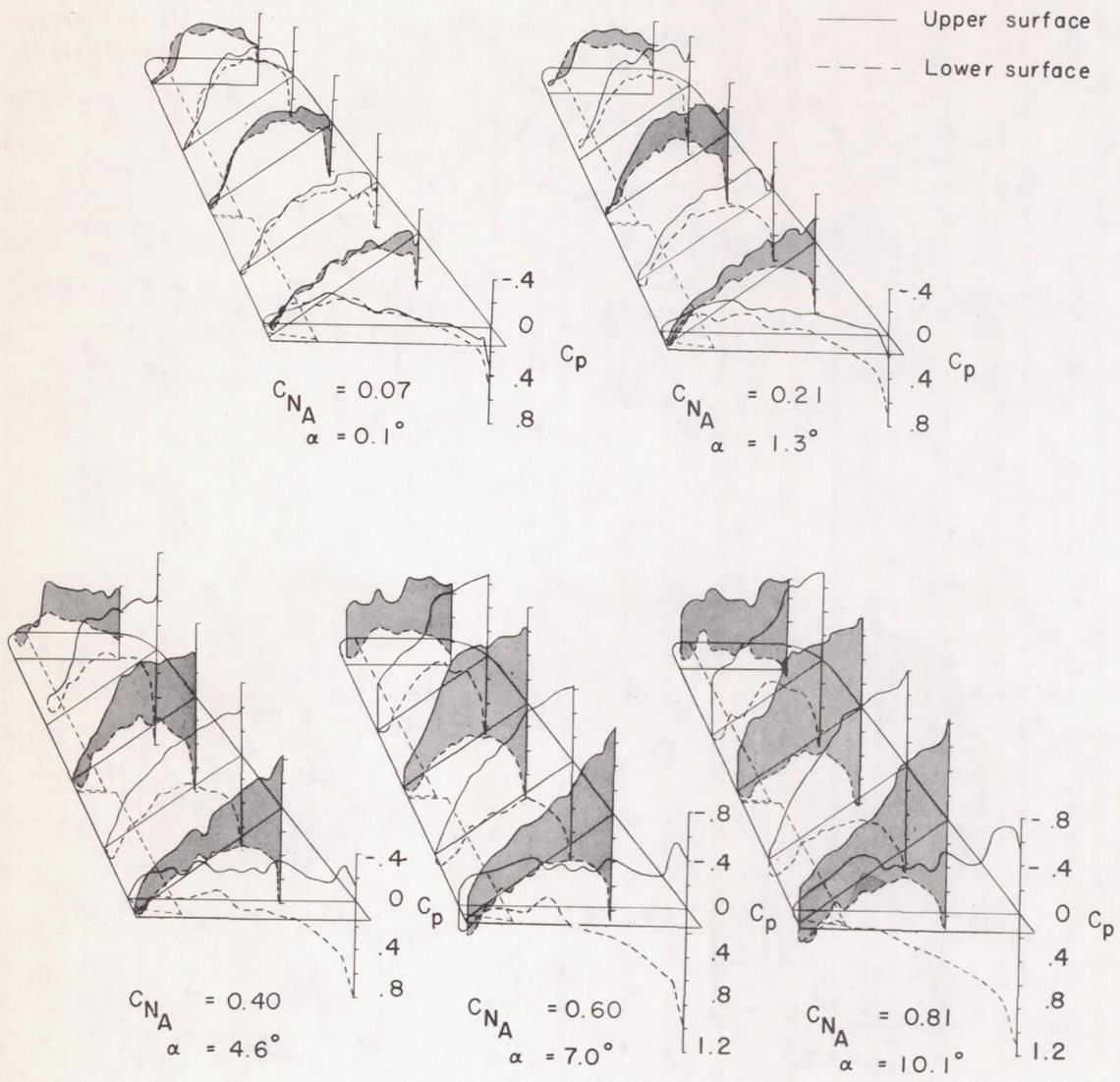
(b) M ≈ 0.90.

Figure 4.- Continued.



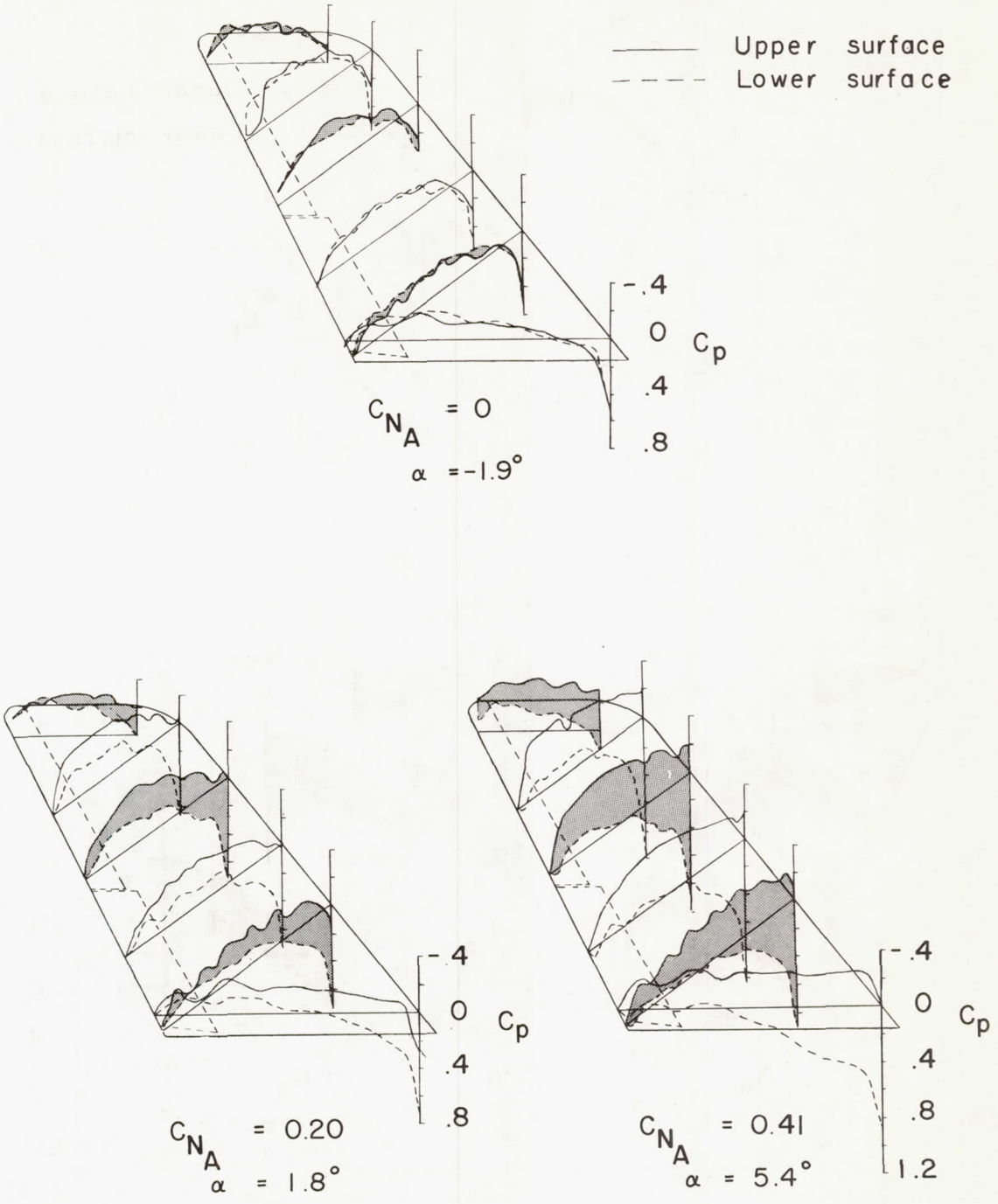
(c) M ≈ 1.00.

Figure 4.- Continued.



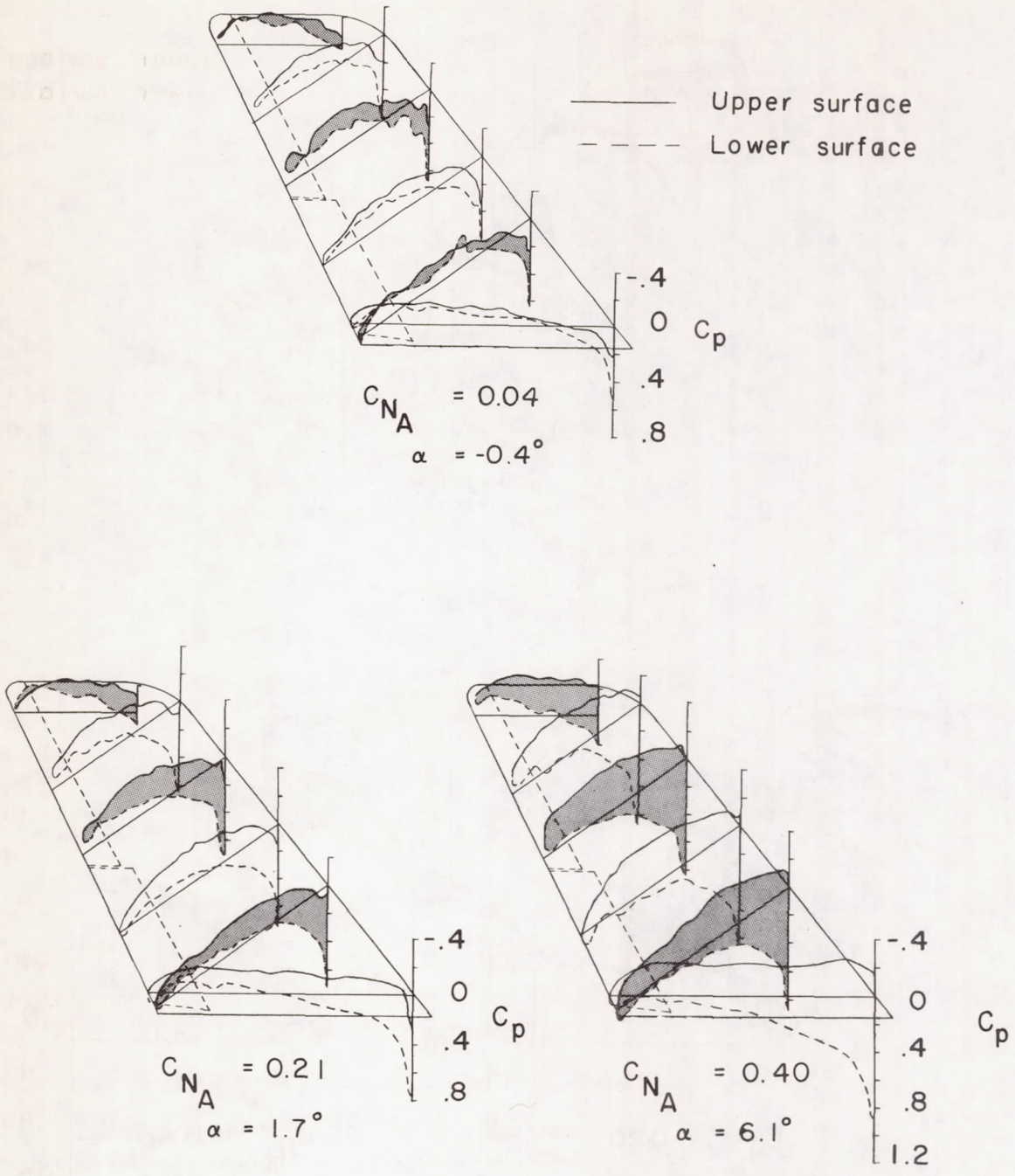
(d) M ≈ 1.13.

Figure 4.- Continued.



(e) M ≈ 1.48.

Figure 4.- Continued.



(f) M ≈ 1.73.

Figure 4.- Concluded.

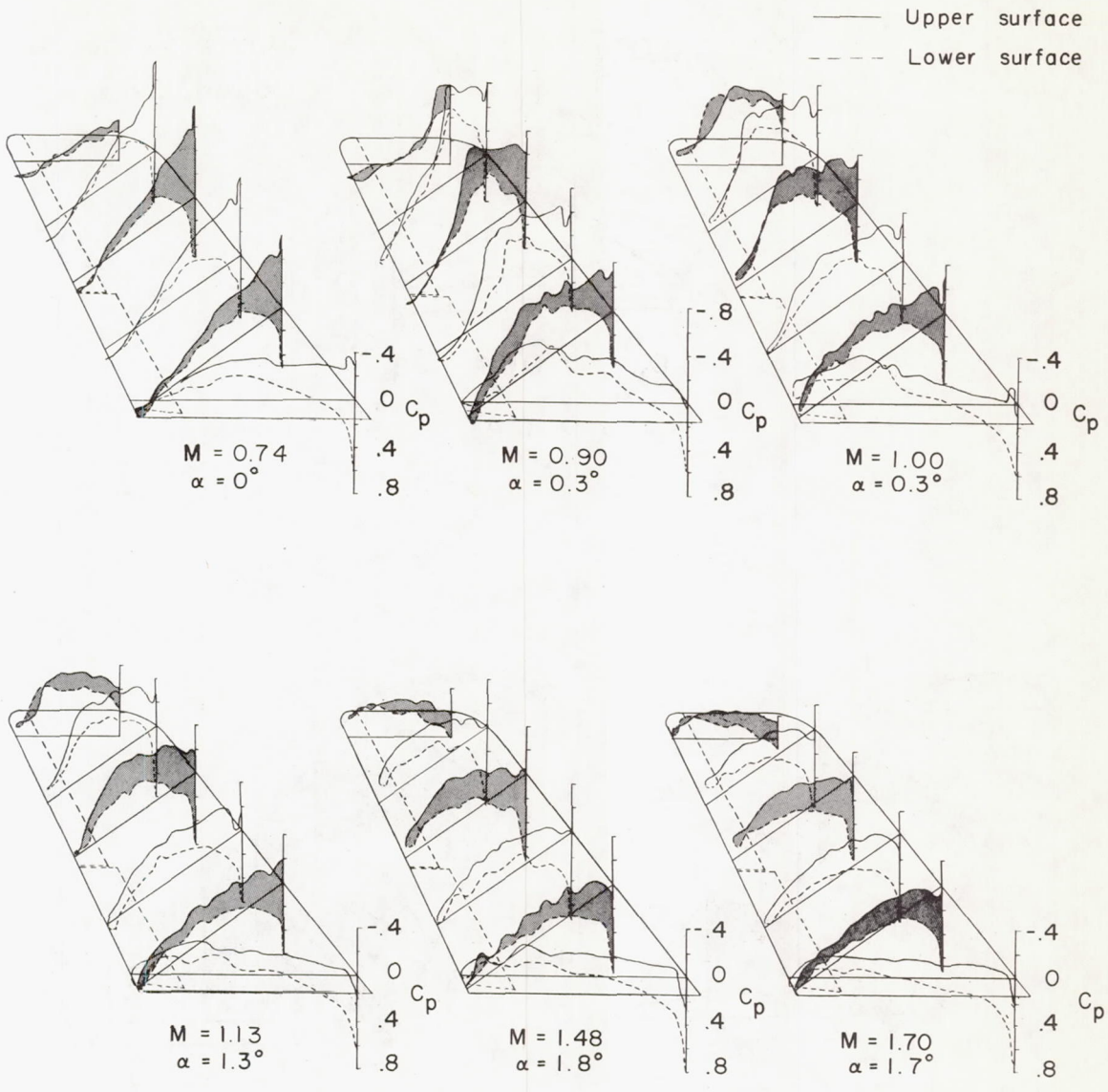
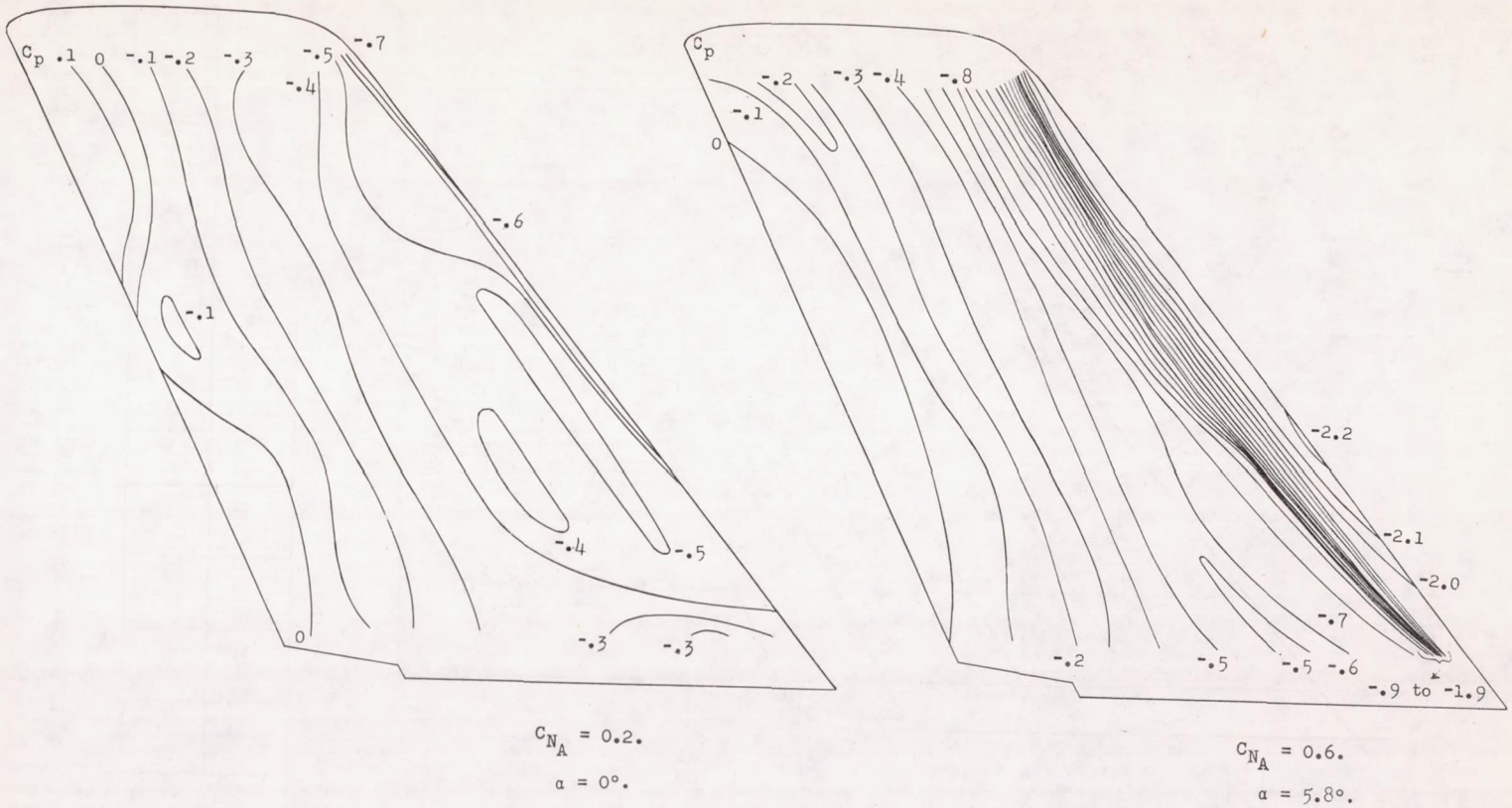
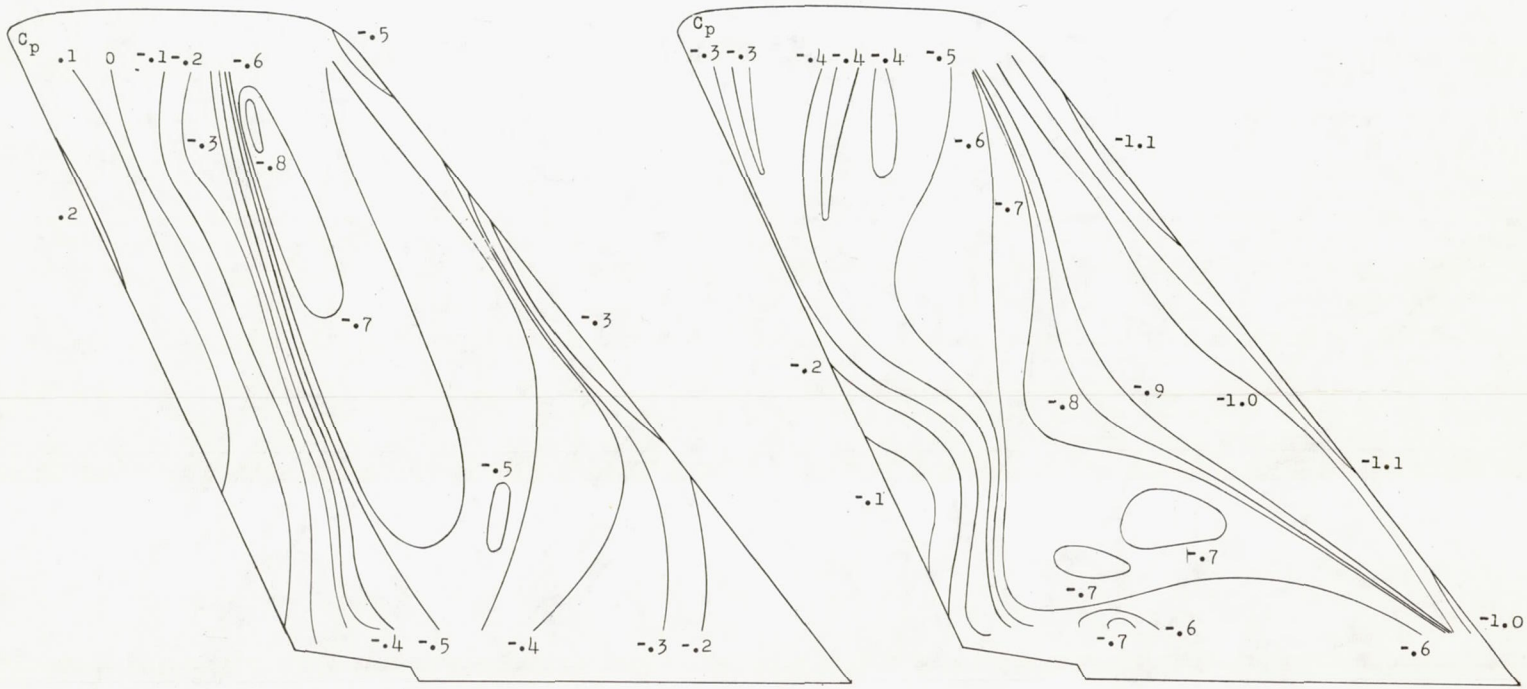


Figure 5.- Wing plan views showing the effect of Mach number on the D-558-II wing pressure distributions at an airplane normal-force coefficient of approximately 0.2.



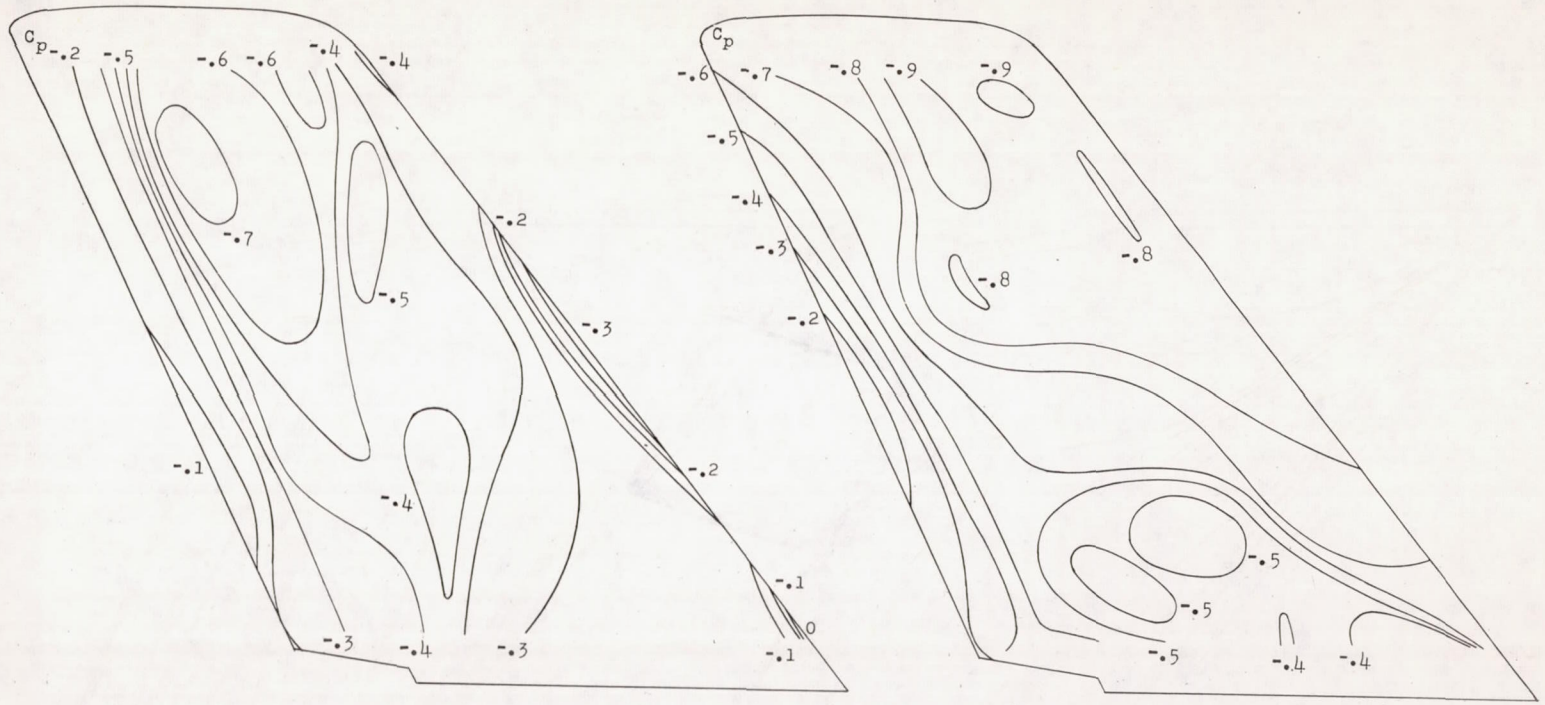
(a) $M \approx 0.73$.

Figure 6.- Pressure contours showing the effect of Mach number and lift on the upper surface of the D-558-II wing.



(b) $M \approx 0.90$.

Figure 6.- Continued.

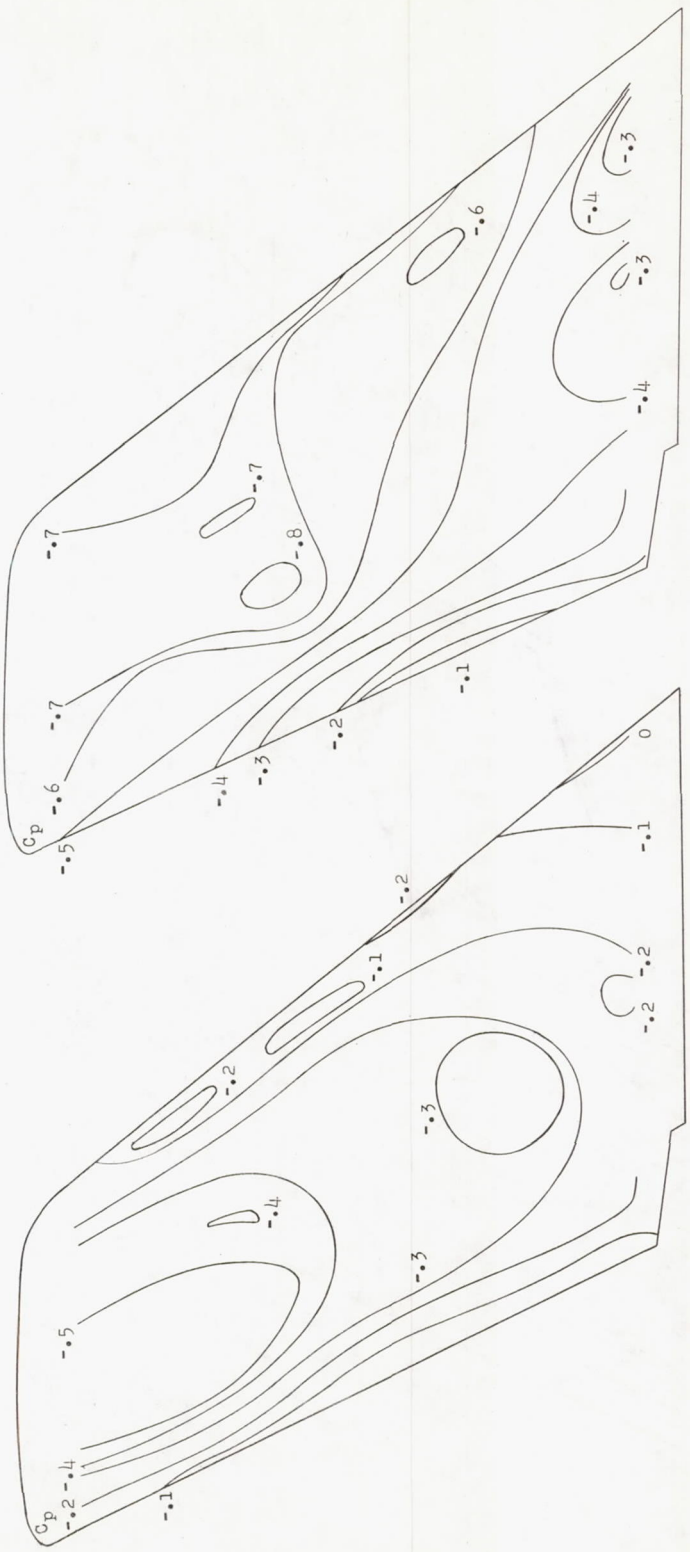


$C_{N_A} = 0.2$.
$\alpha = 0.3°$.

$C_{N_A} = 0.6$.
$\alpha = 6.0°$.

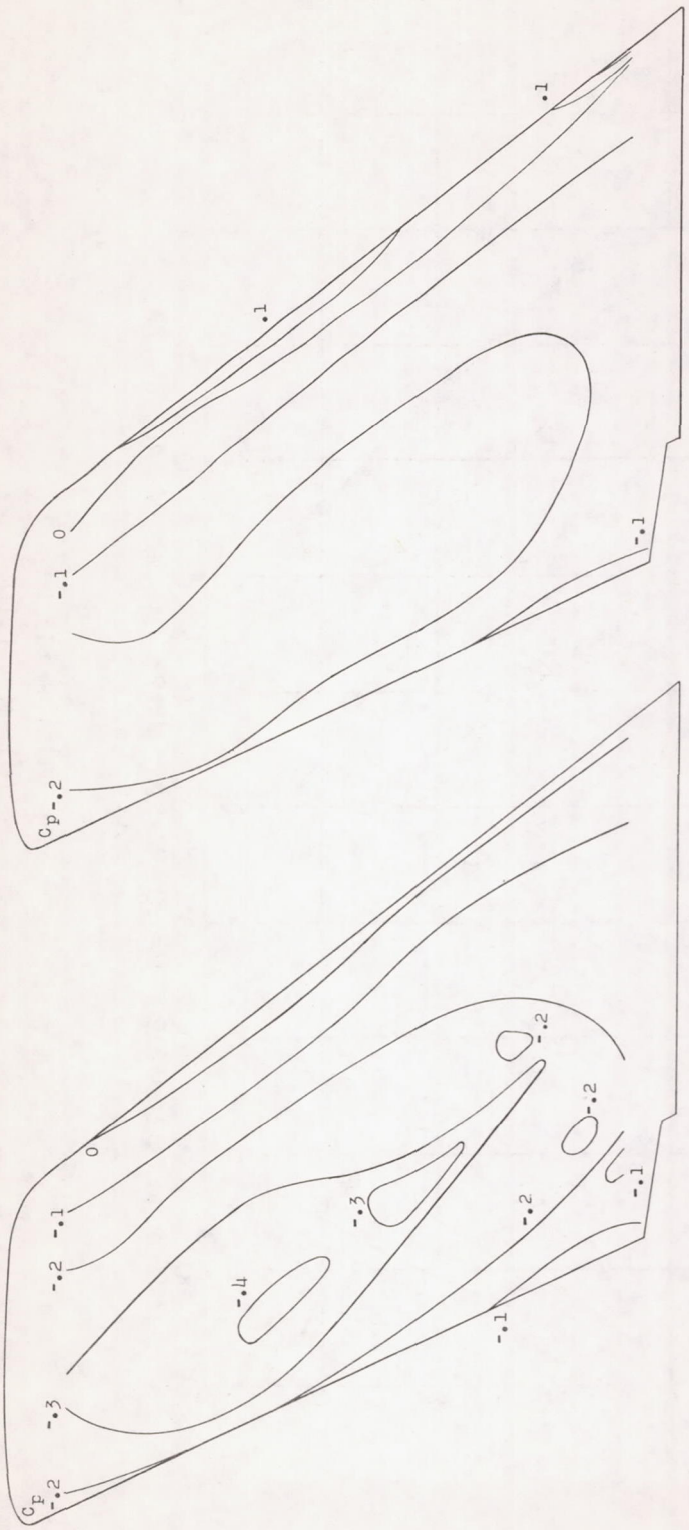
(c) $M \approx 1.00$.

Figure 6.- Continued.



(d) $M \approx 1.10$.

Figure 6.- Continued.

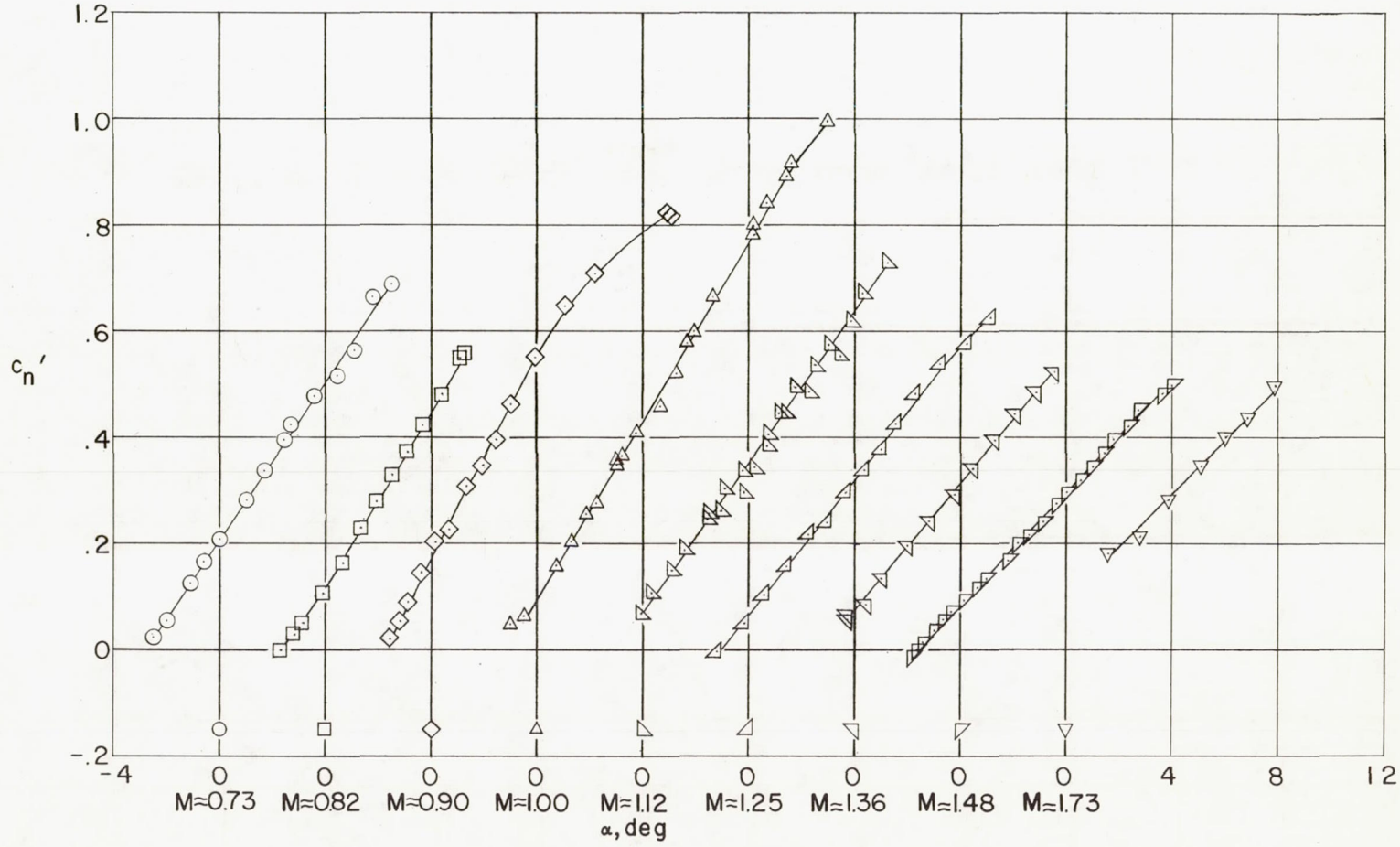


$M \approx 1.48$.
$C_{N_A} = 0.2$.
$\alpha = 1.8°$.

$M \approx 1.73$.
$C_{N_A} = 0.2$.
$\alpha = 1.7°$.

(e) M as noted.

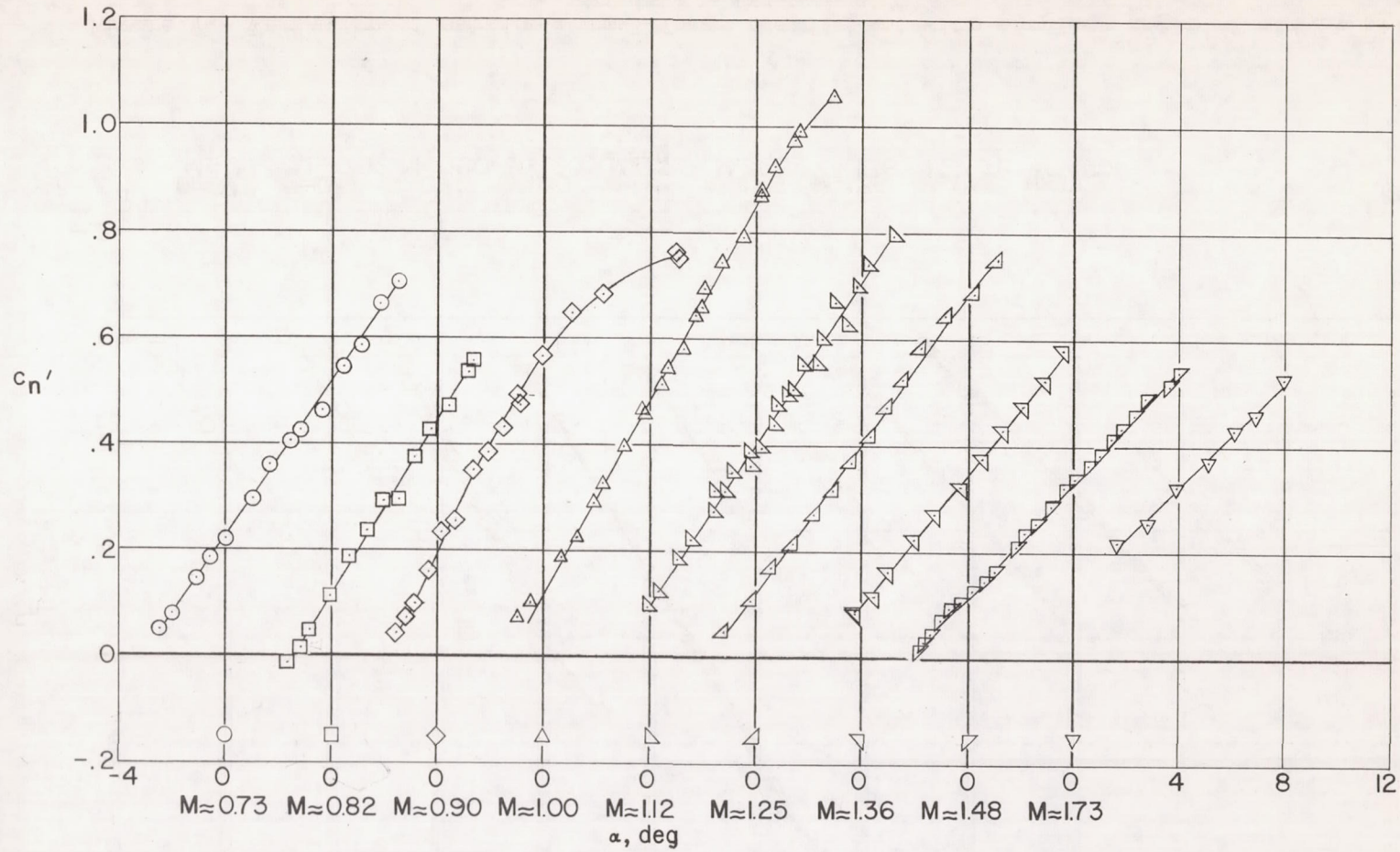
Figure 6.- Concluded.



(a) Row 1.

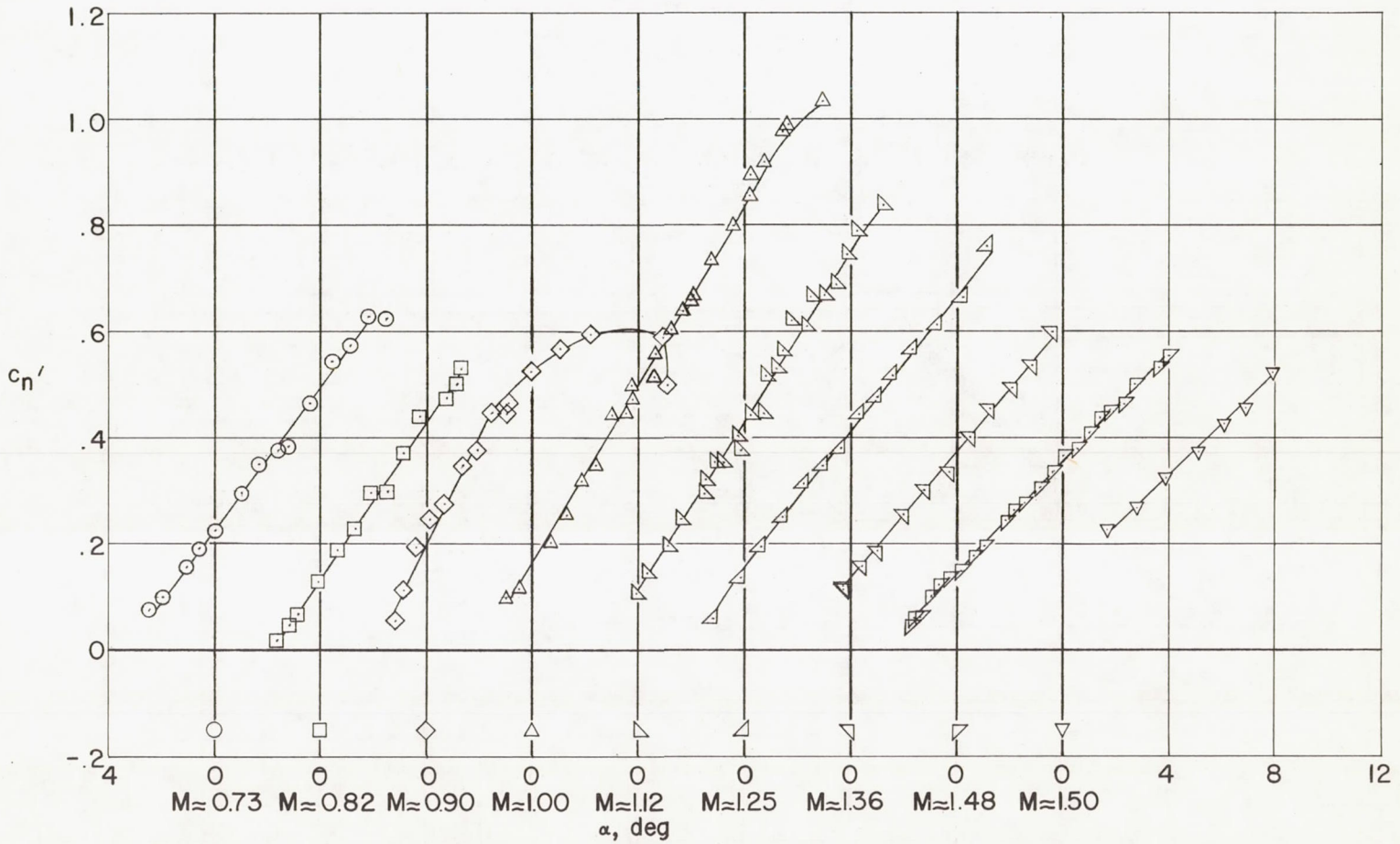
Figure 7.- Variation of section normal-force coefficient with airplane angle of attack at selected Mach numbers.

CONFIDENTIAL



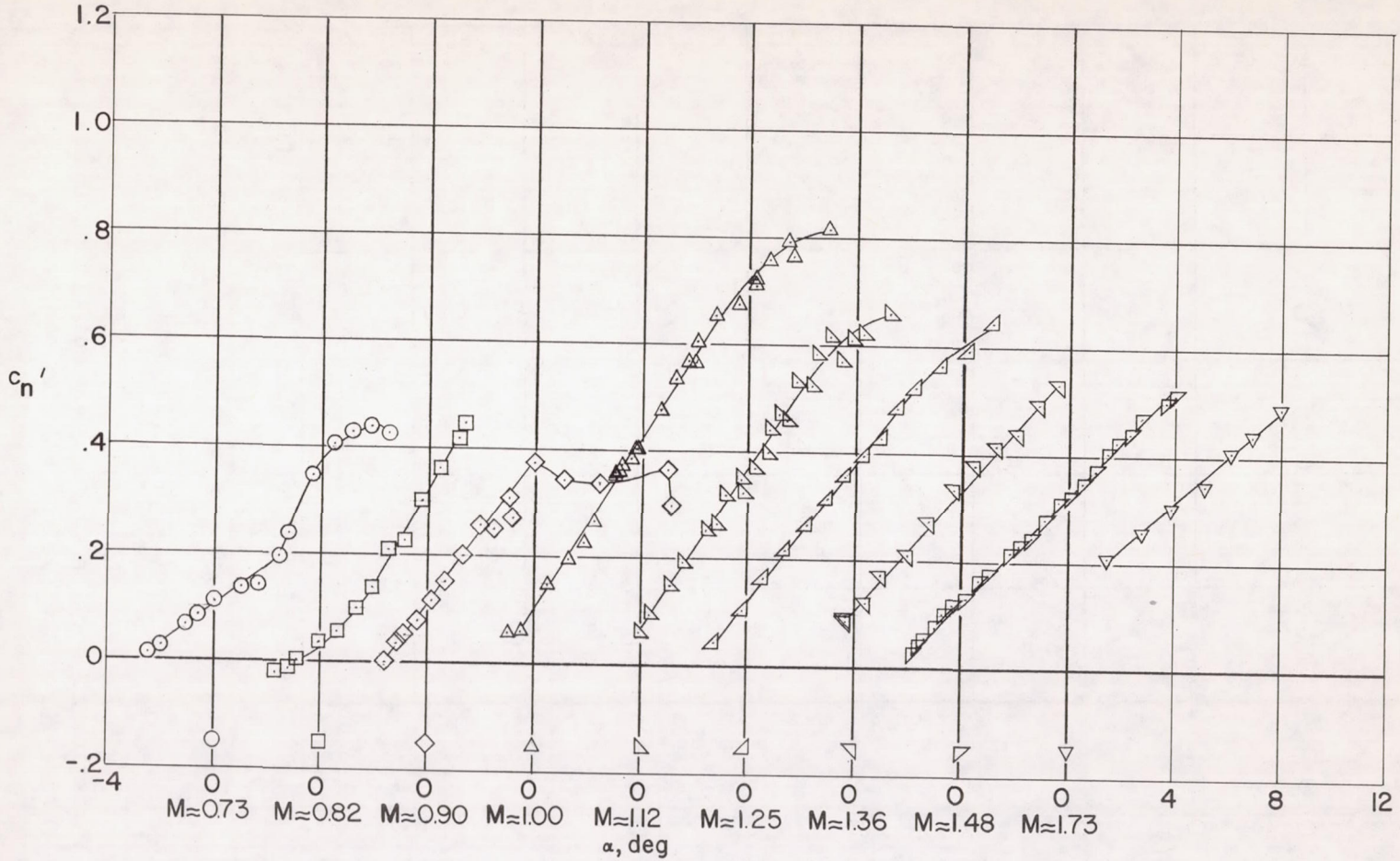
(b) Row 2.

Figure 7.- Continued.



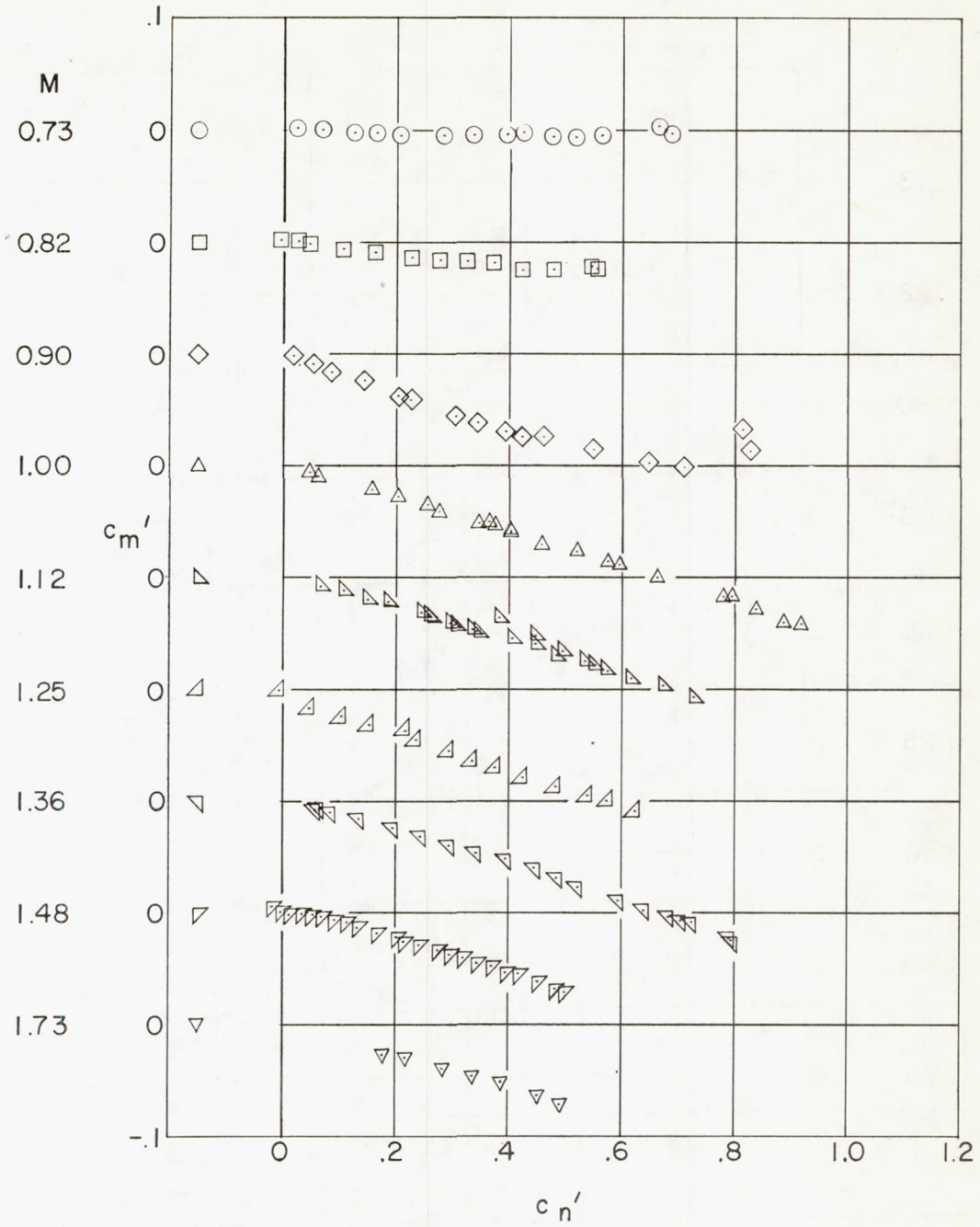
(c) Row 3.

Figure 7.- Continued.



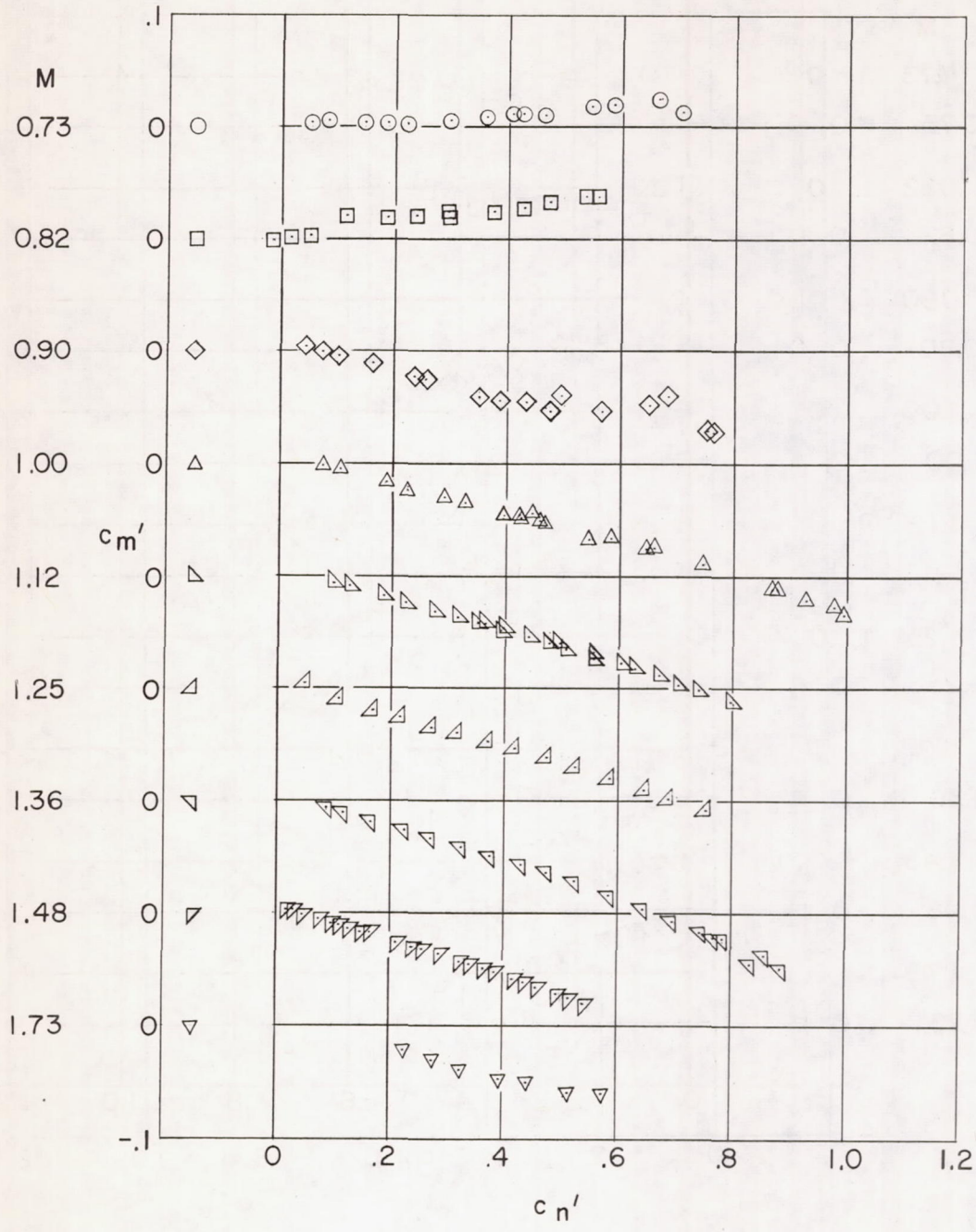
(d) Row 4.

Figure 7.- Concluded.



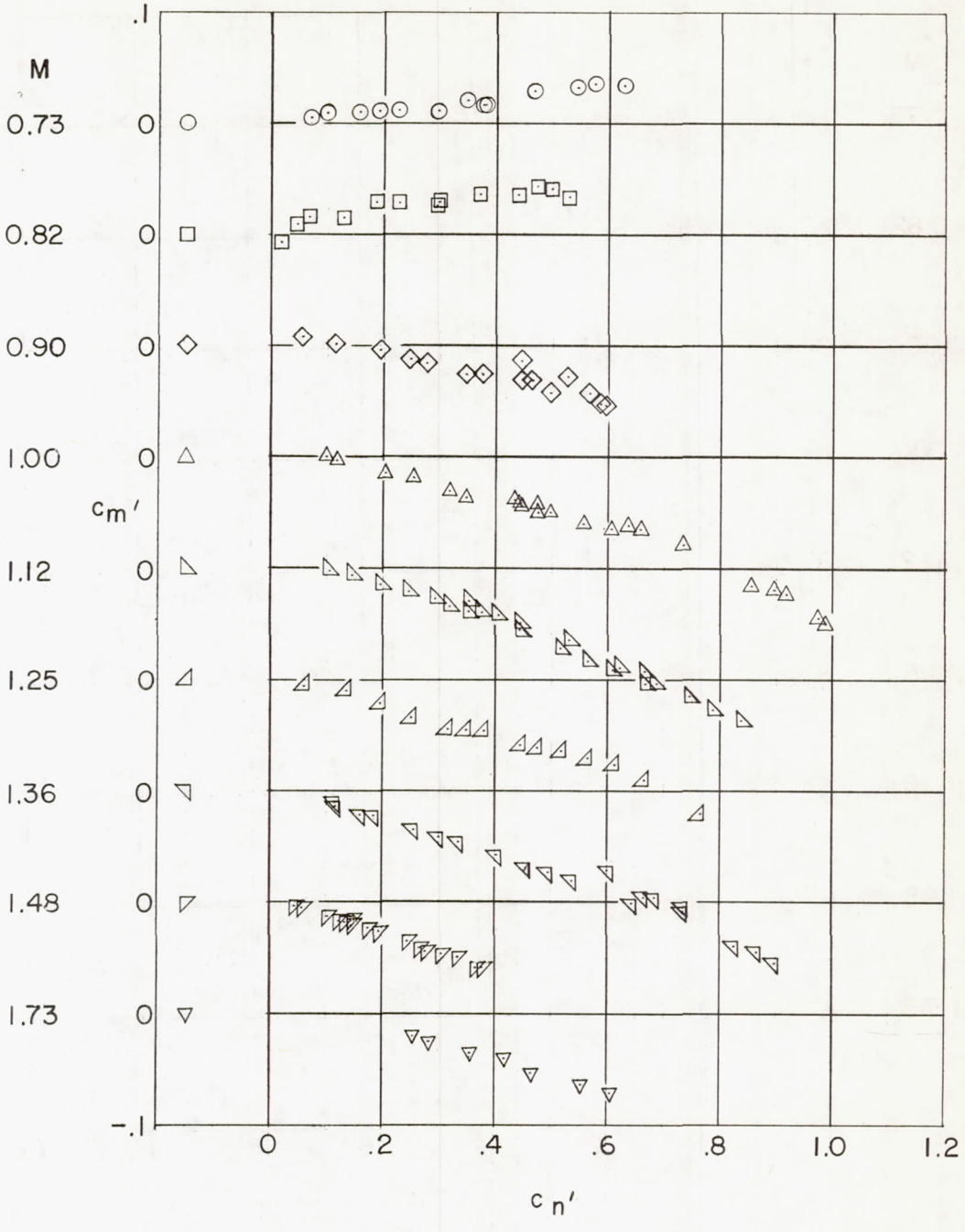
(a) Row 1.

Figure 8.- Variation of section pitching-moment coefficient with section normal-force coefficient at selected Mach numbers.



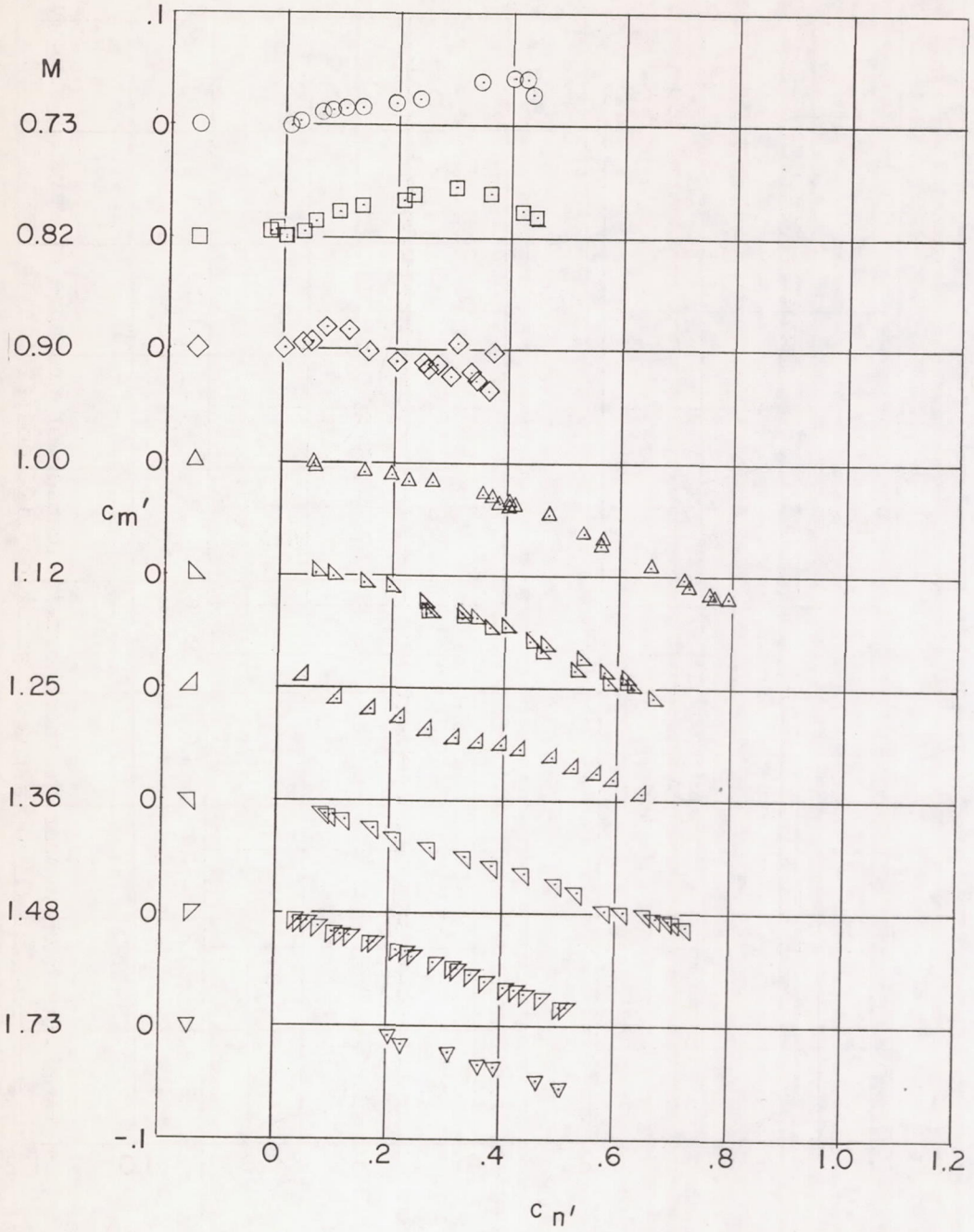
(b) Row 2.

Figure 8.- Continued.



(c) Row 3.

Figure 8.- Continued.



(d) Row 4.

Figure 8.- Concluded.

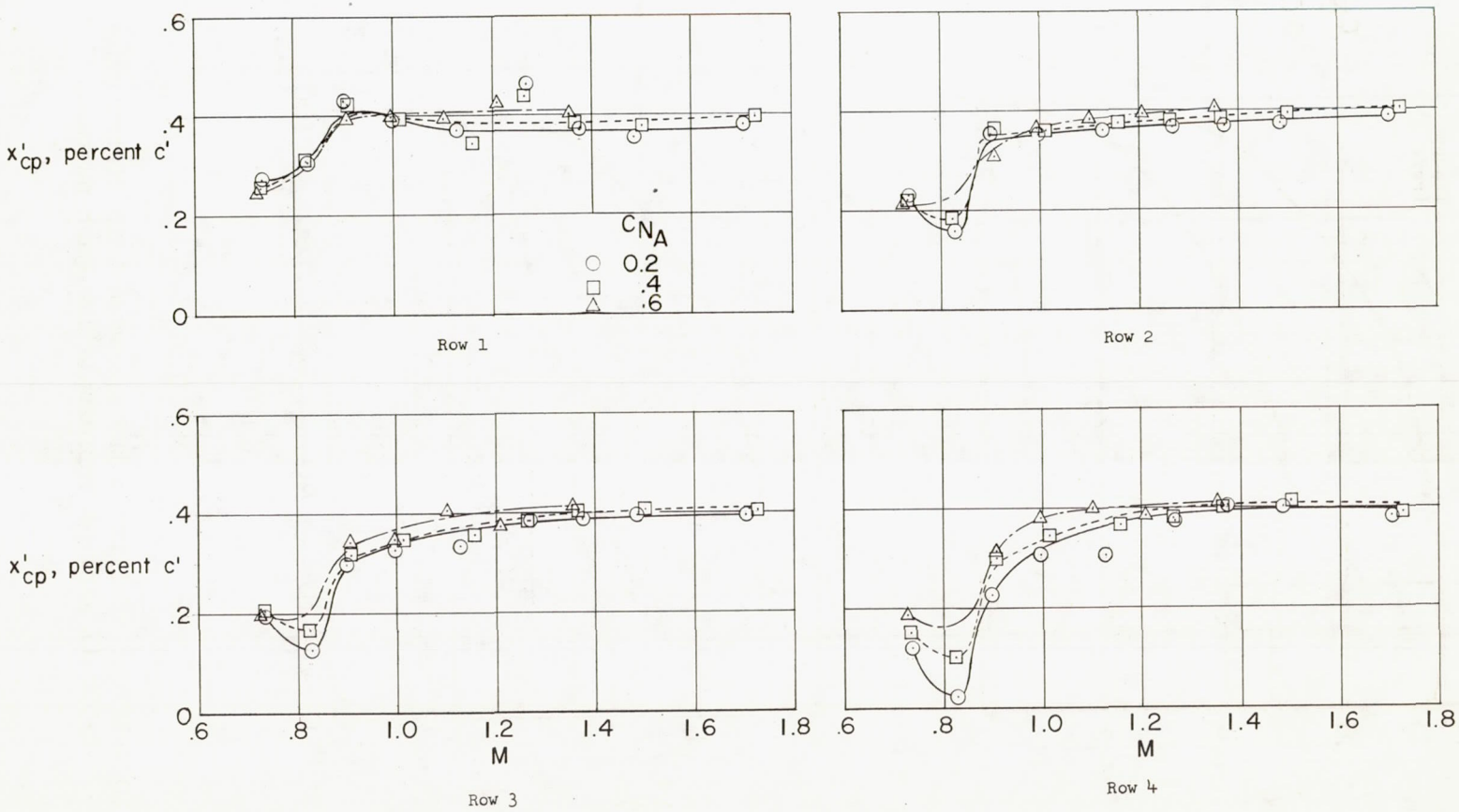
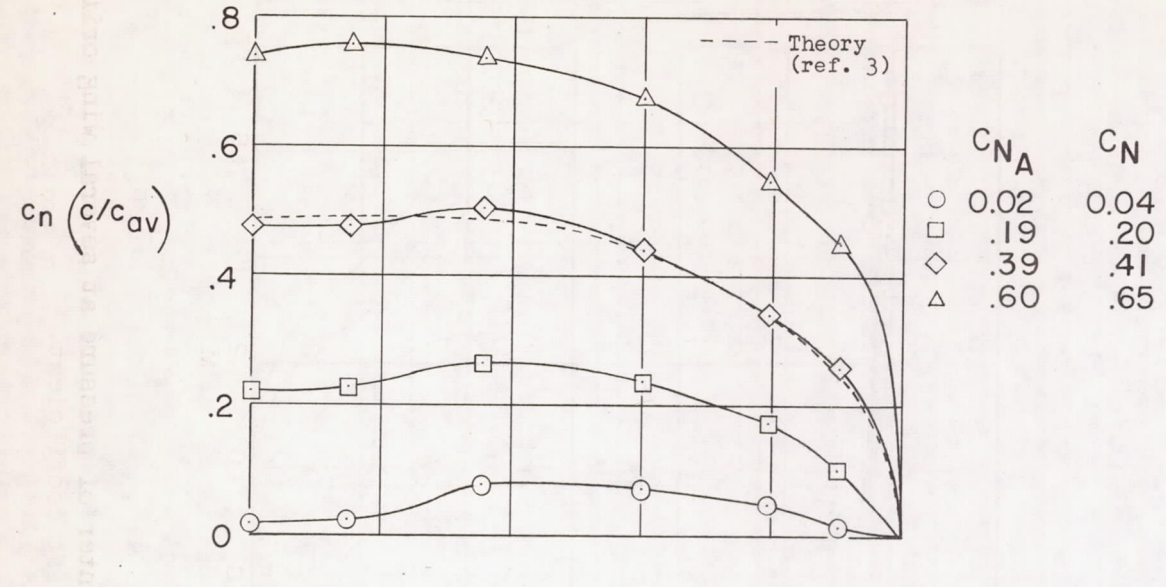
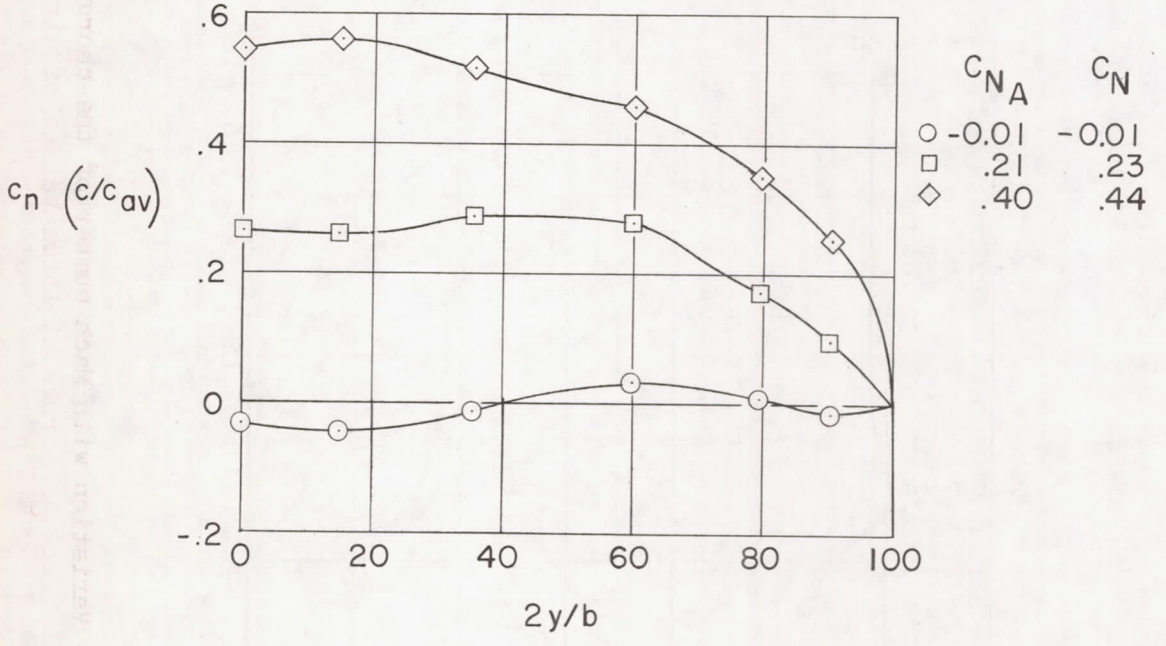


Figure 9.- Variation with Mach number of the chordwise center of pressure at several wing orifice rows at three values of airplane lift coefficient.

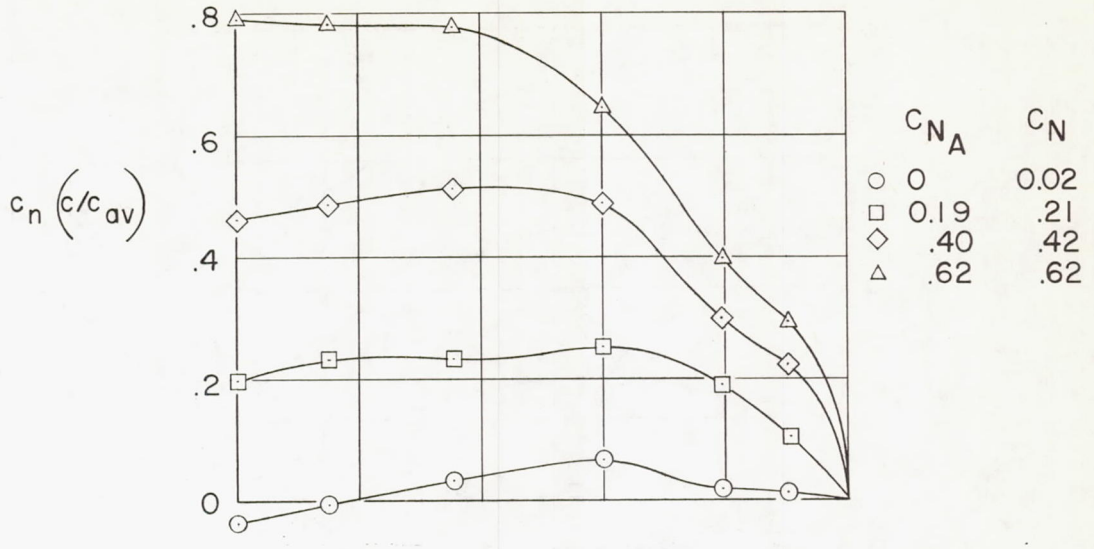


(a) $M \approx 0.73$.

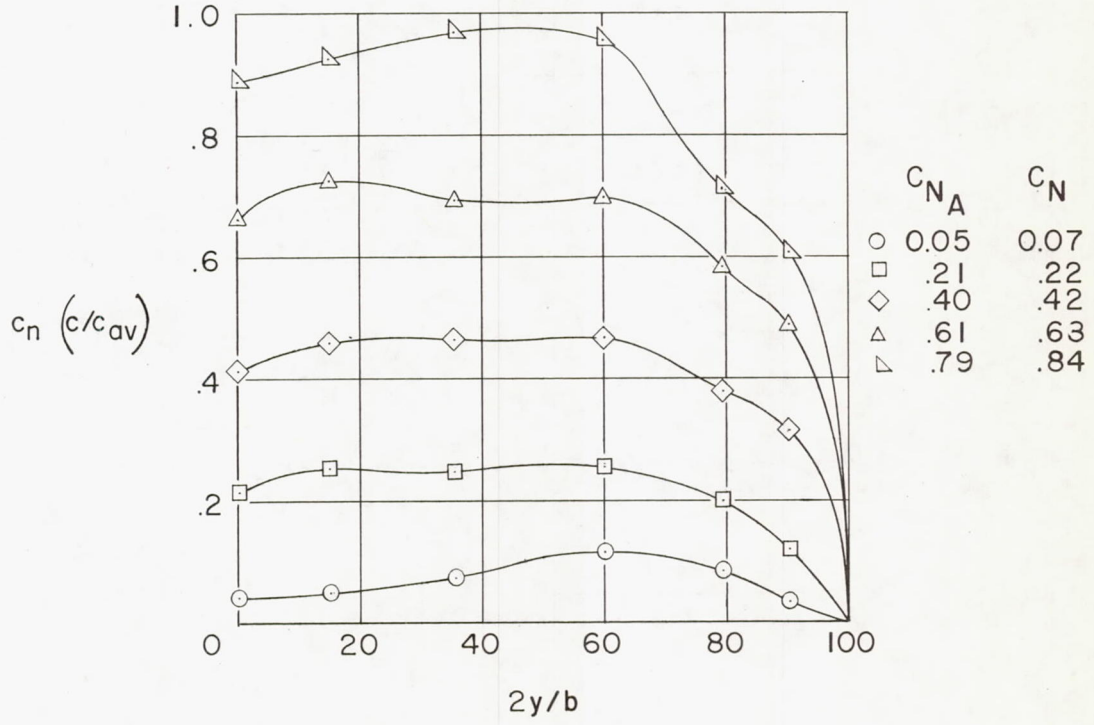


(b) $M \approx 0.82$.

Figure 10.- Effect of lift on the spanwise load distribution of the D-558-II wing at representative Mach numbers.

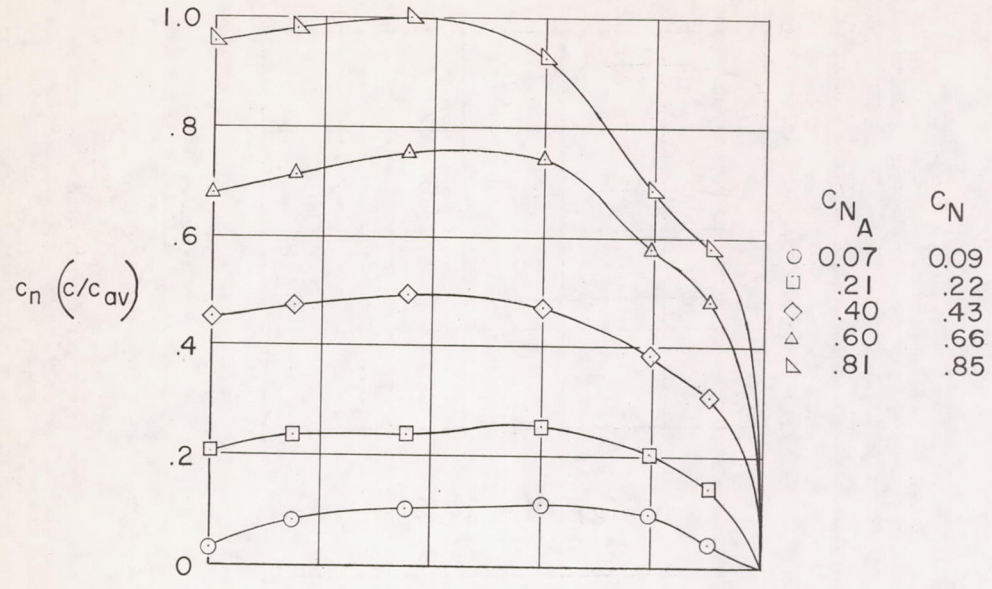


(c) M ≈ 0.90.

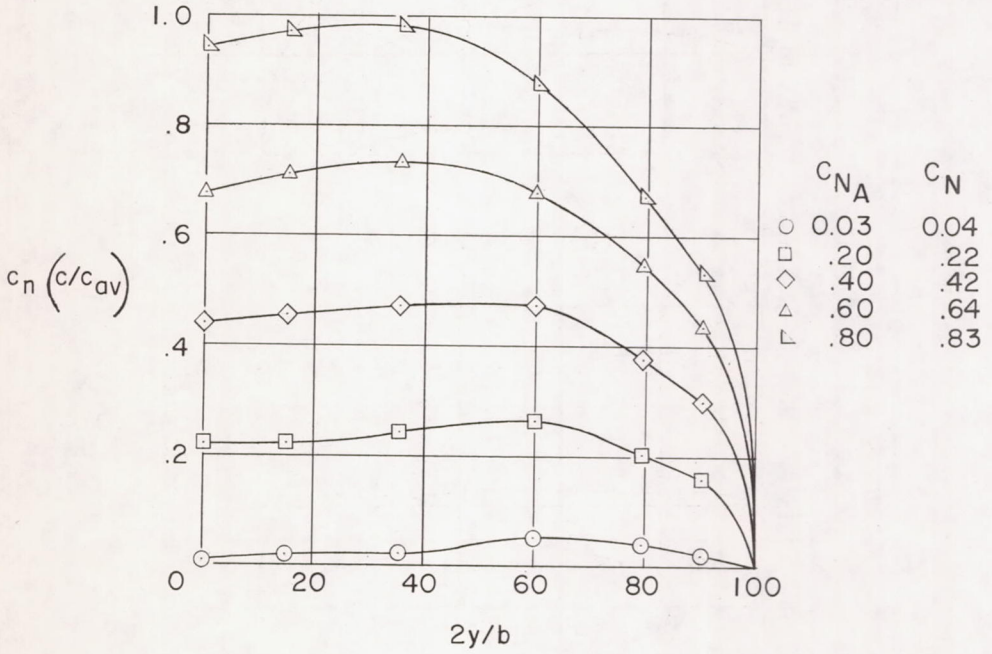


(d) M ≈ 1.00.

Figure 10.- Continued.

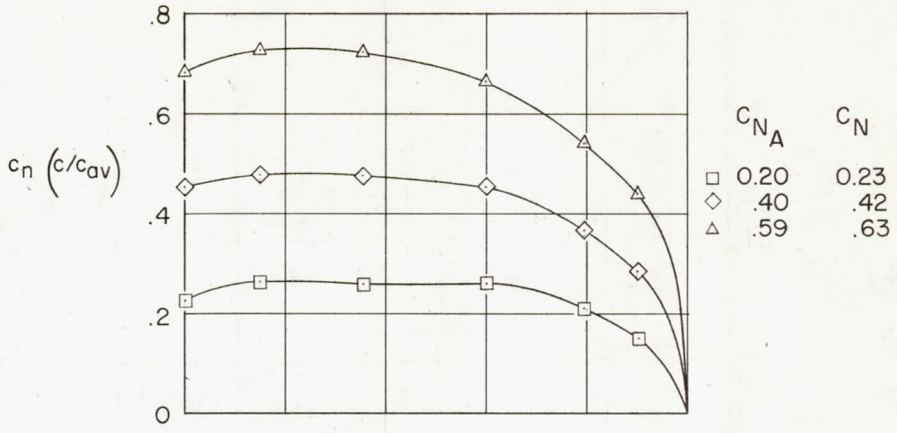


(e) $M \approx 1.12$.

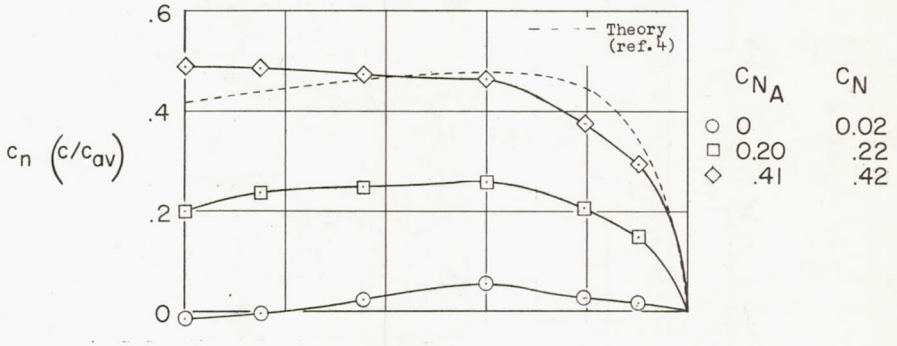


(f) $M \approx 1.25$.

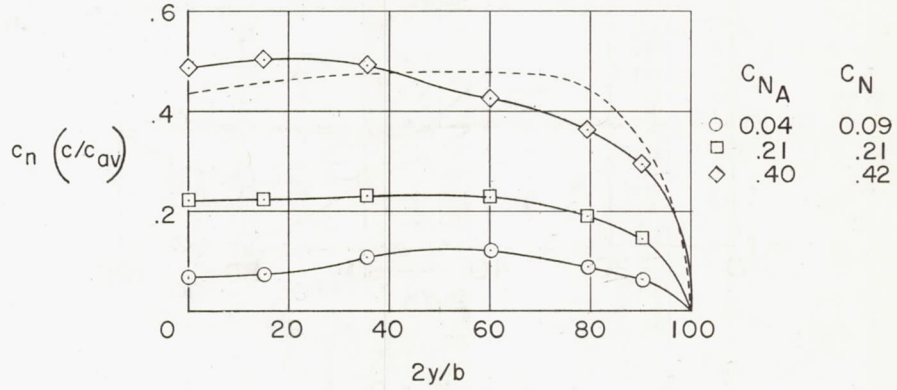
Figure 10.- Continued.



(g) M ≈ 1.36.

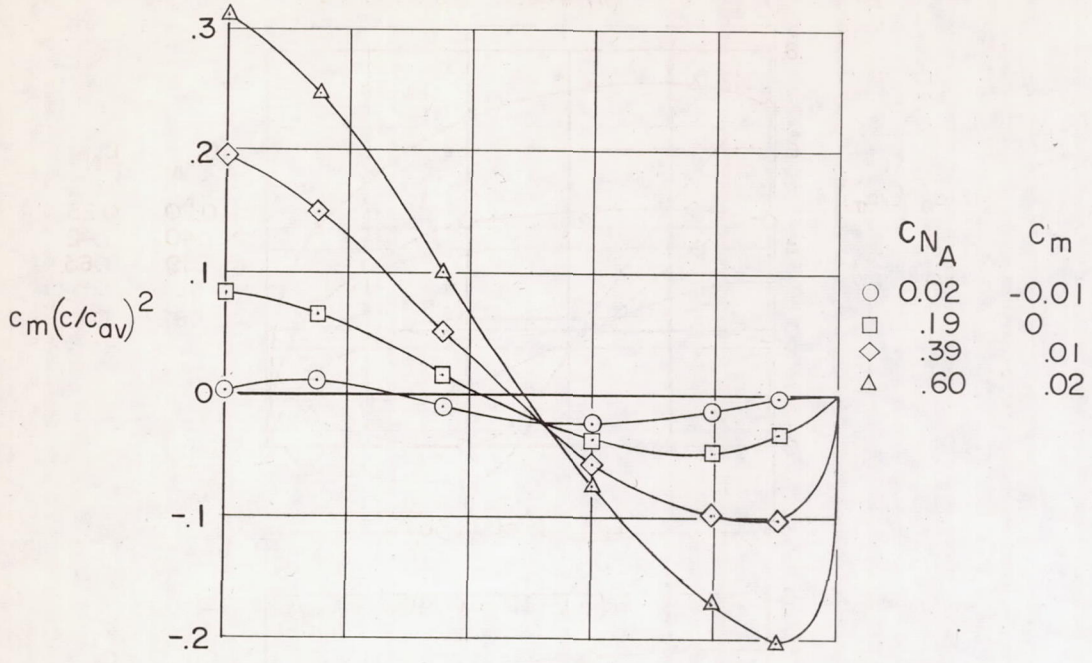


(h) M ≈ 1.48.

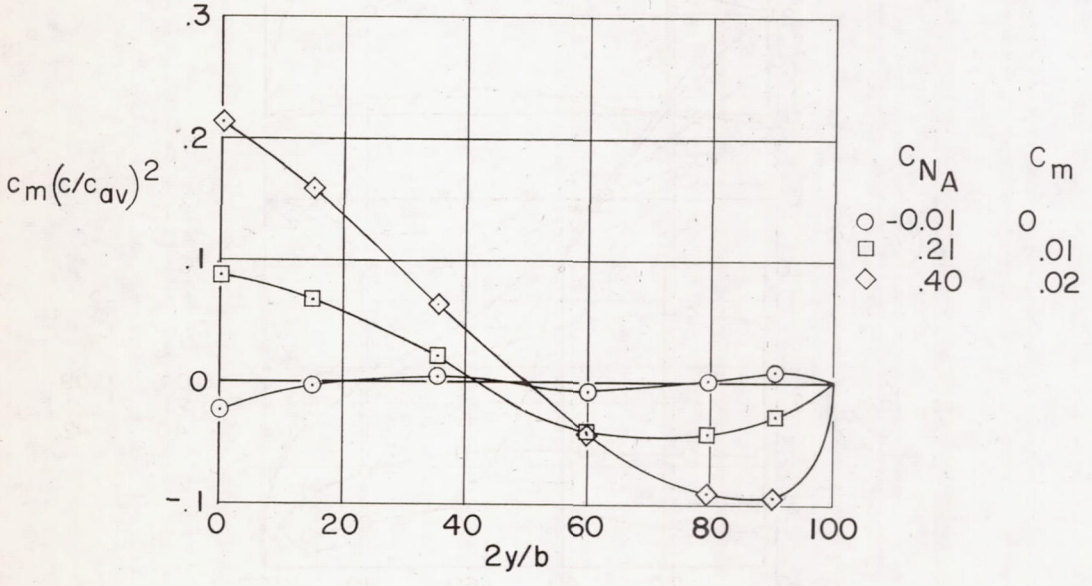


(i) M ≈ 1.73.

Figure 10.- Concluded.

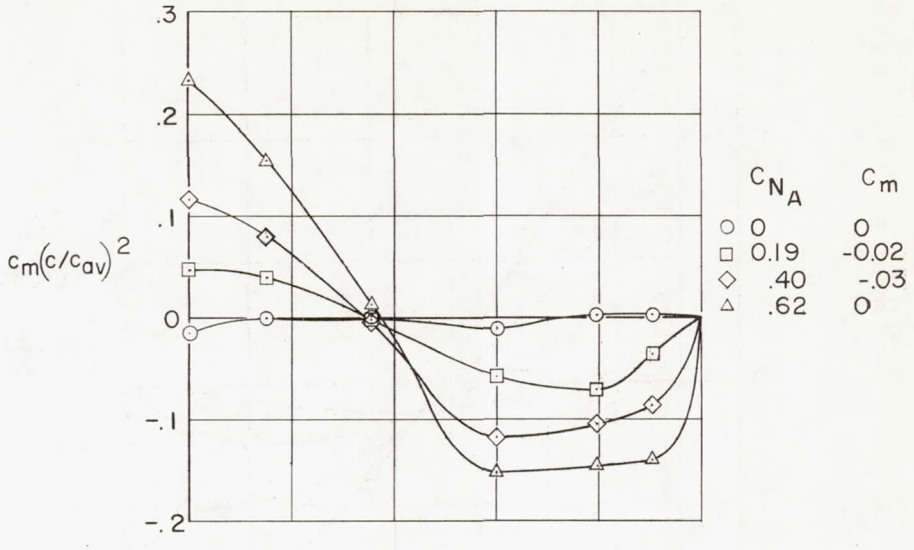


(a) M ≈ 0.73.

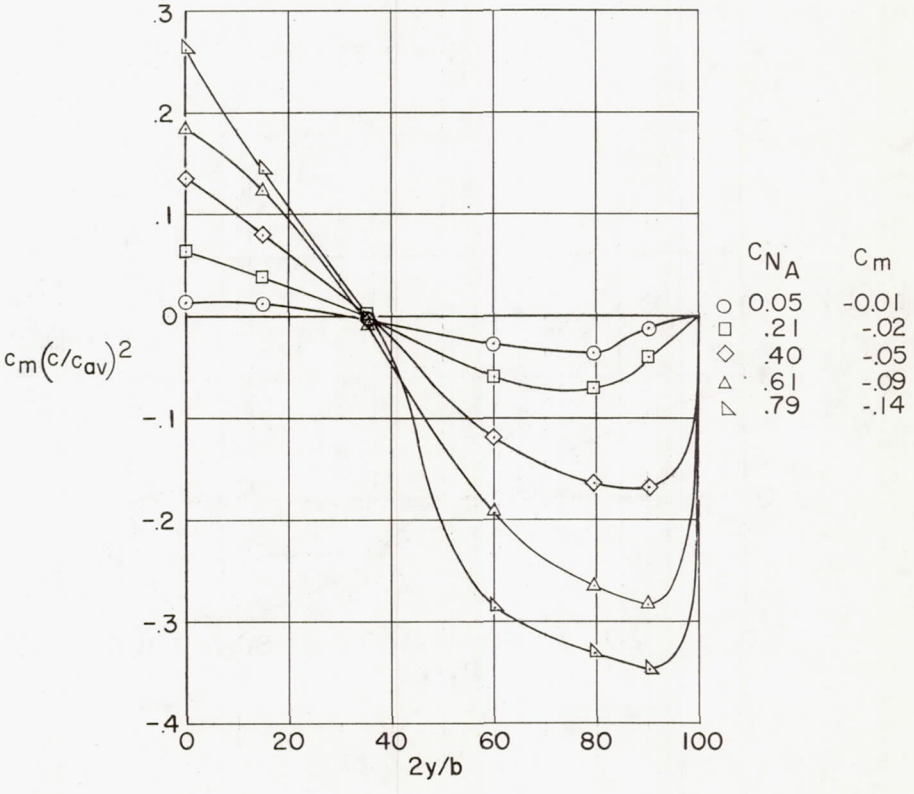


(b) M ≈ 0.82.

Figure 11.- Effect of lift on the spanwise pitching-moment distribution of the D-558-II wing at representative Mach numbers.

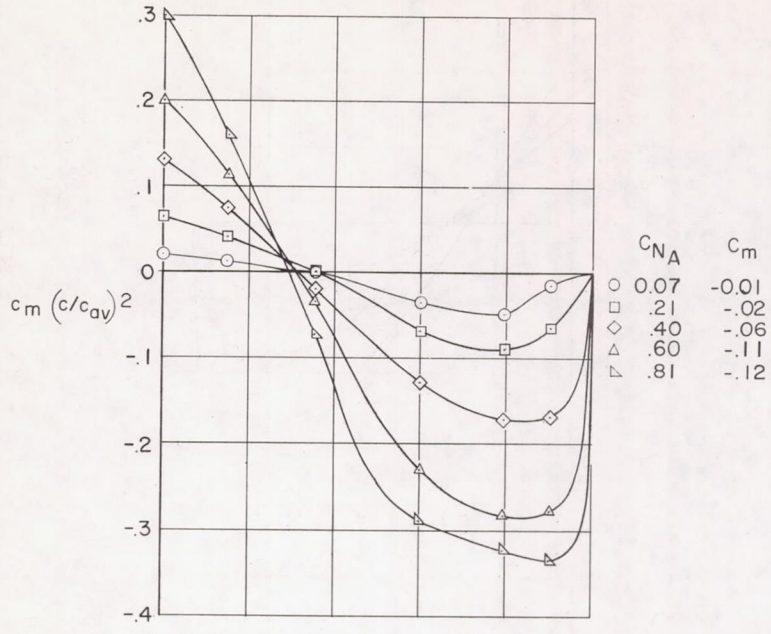


(c) M ≈ 0.90.

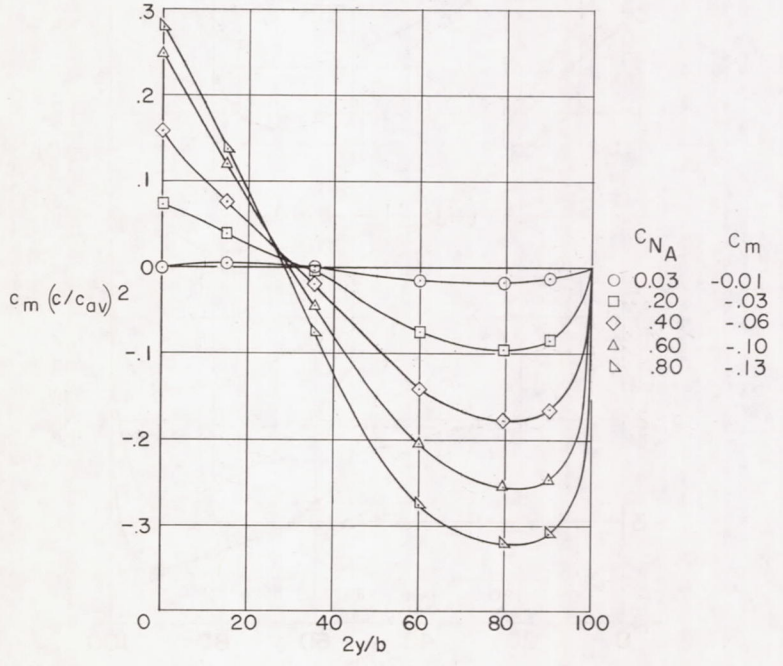


(d) M ≈ 1.00.

Figure 11.- Continued.

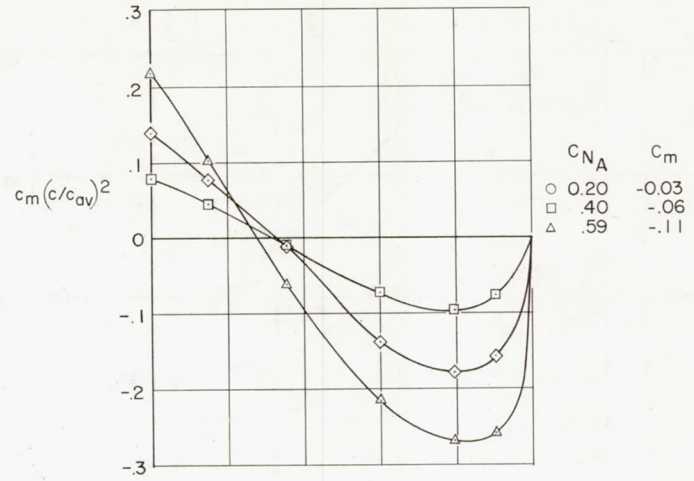


(e) $M \approx 1.12$.

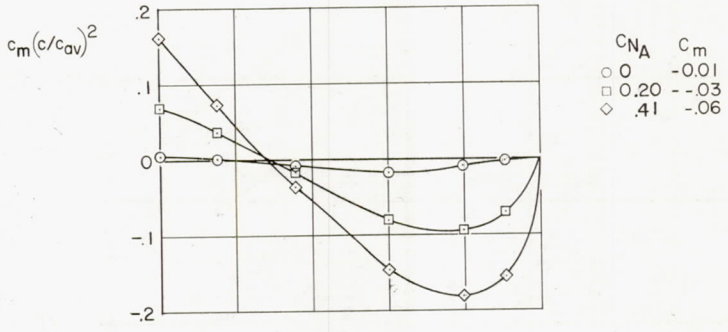


(f) $M \approx 1.25$.

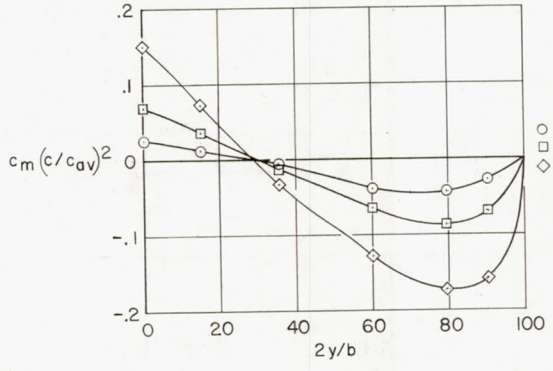
Figure 11.- Continued.



(g) M ≈ 1.36.



(h) M ≈ 1.48.



(i) M ≈ 1.73.

Figure 11.- Concluded.

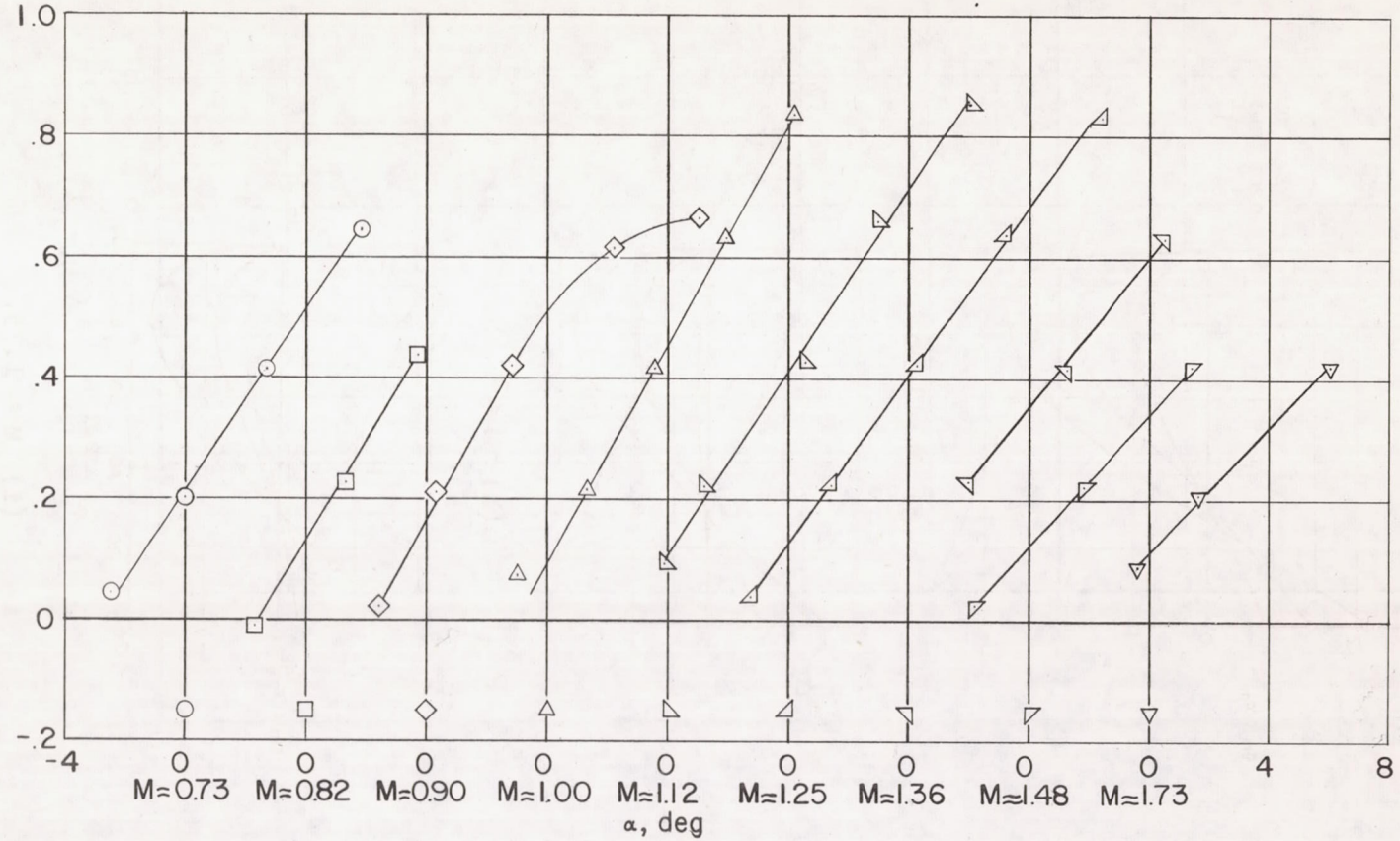


Figure 12.- Variation of wing-panel normal-force coefficient with airplane angle of attack at selected Mach numbers.

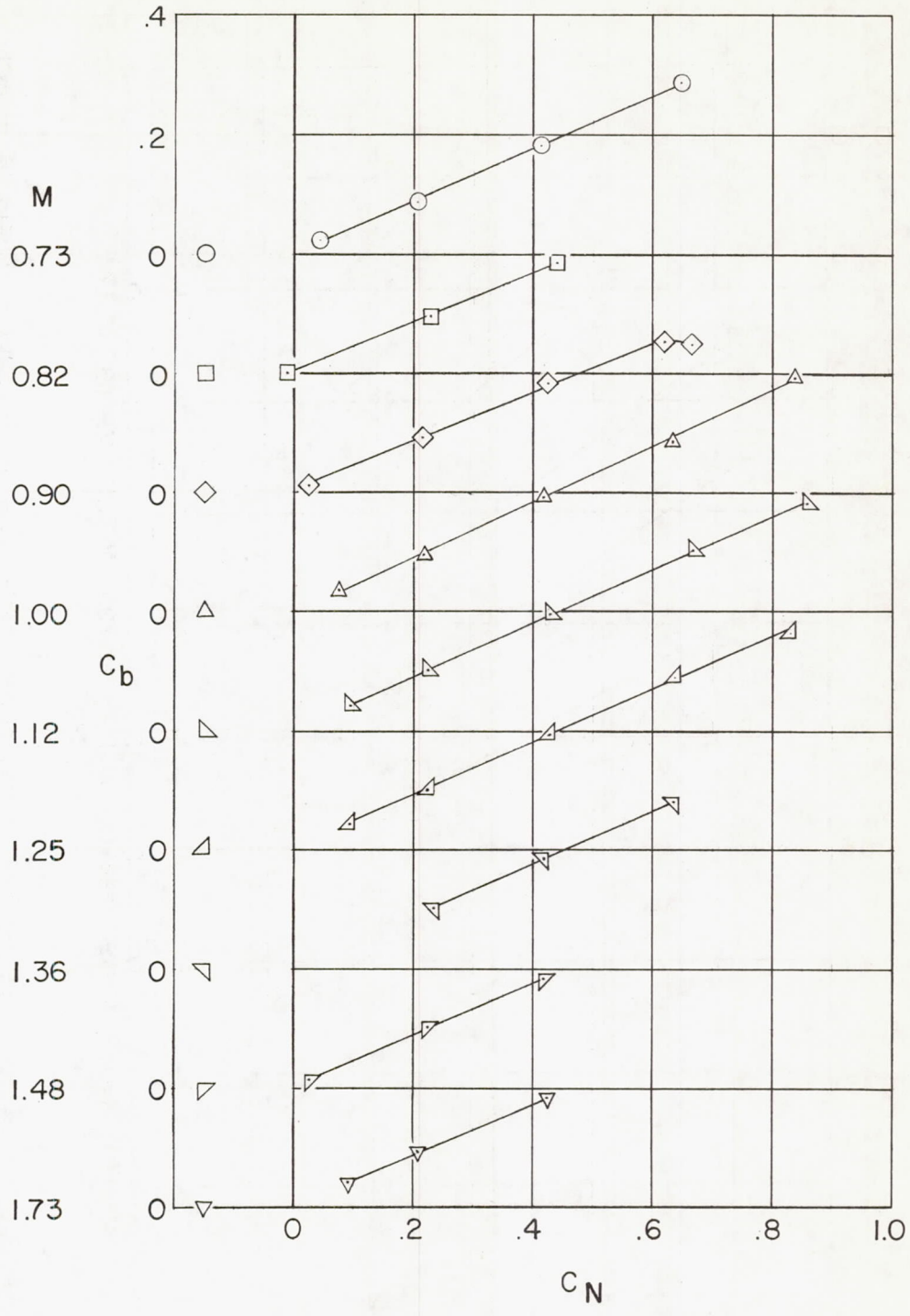


Figure 13.- Variation of wing-panel normal-force coefficient with panel bending-moment coefficient at selected Mach numbers.

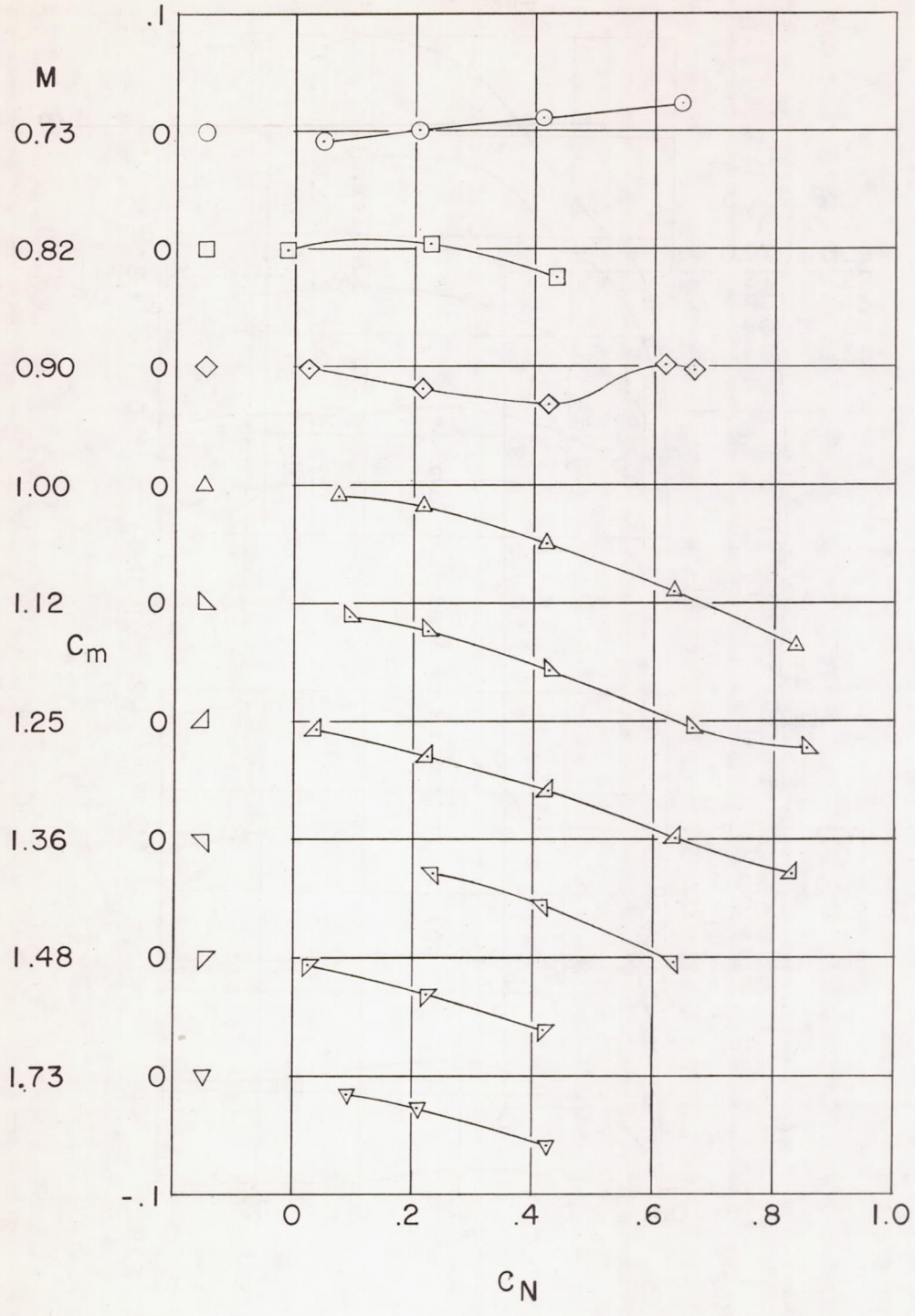
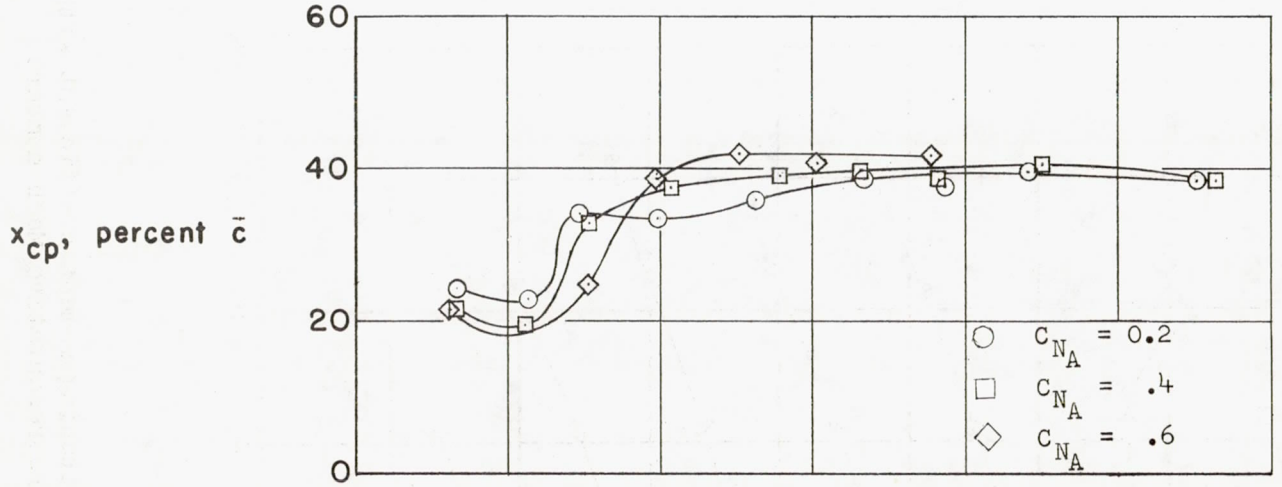
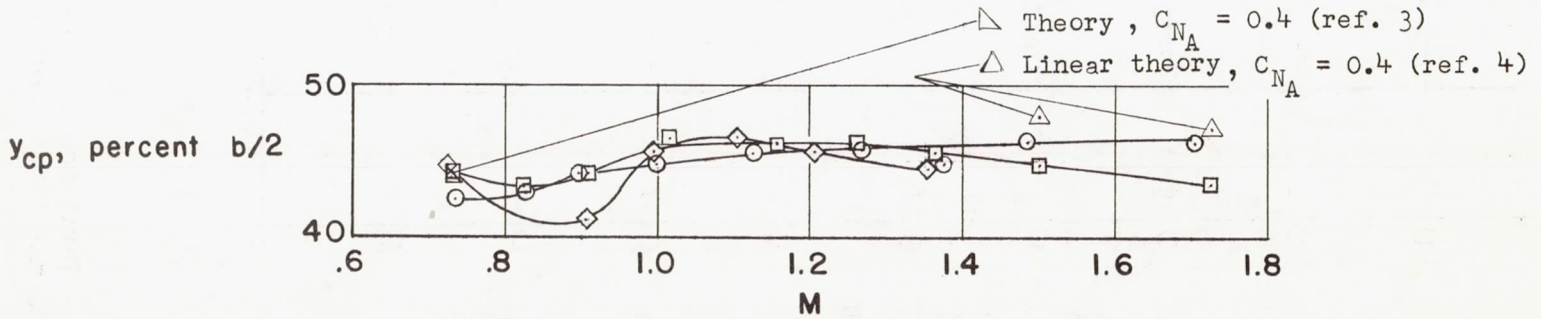


Figure 14.- Variation of wing-panel pitching-moment coefficient with panel normal-force coefficient at representative Mach numbers.



(a) x_{cp} plotted against Mach number.



(b) y_{cp} plotted against Mach number.

Figure 15.- Effect of Mach number and lift on the chordwise and spanwise location of the center of pressure of the D-558-II wing.

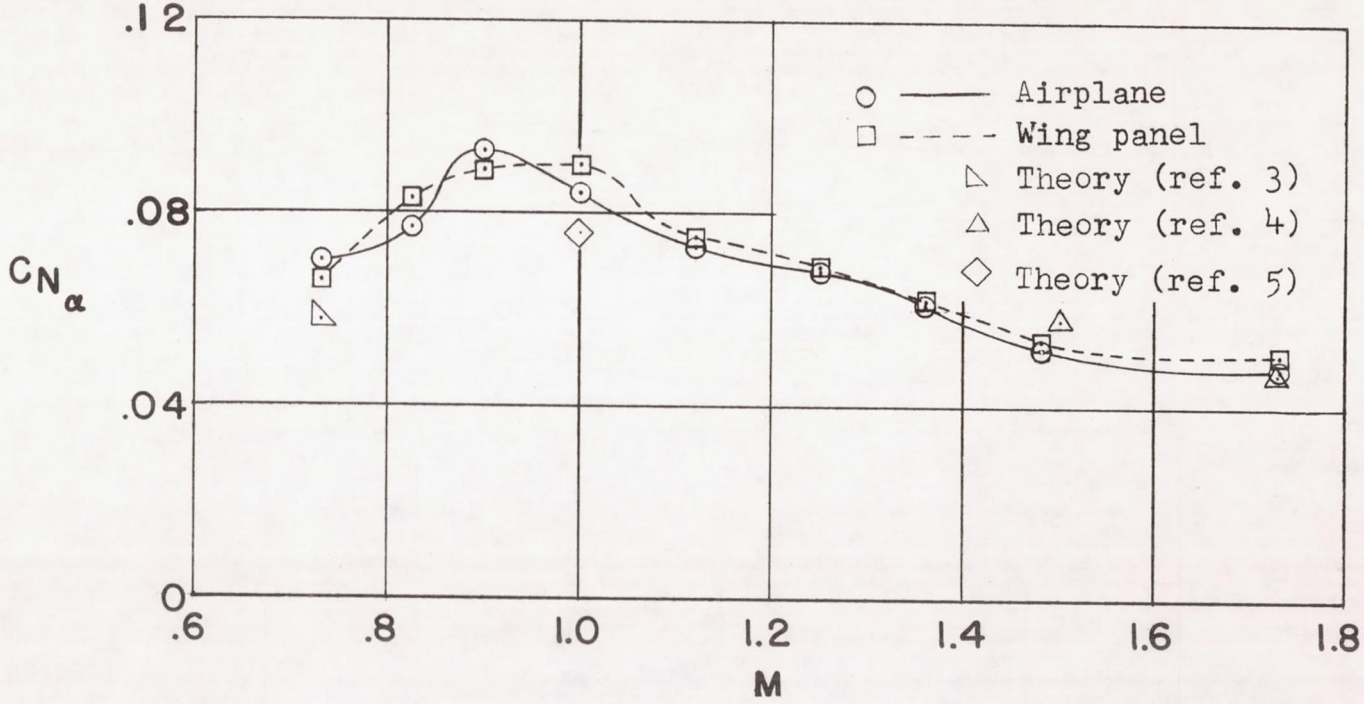


Figure 16.- Variation of the normal-force-curve slopes with Mach number for the wing panel and the airplane.

NACA - Langley Field, V